NOVA SCHOOL OF
SCIENCE & TECHNOLOGY

DEPARTAMENT OF
MATERIALS SCIENCE

CAROLINA DOS SANTOS PARREIRA

BSc in Micro and Nanotechnologies Engineering

Integration of a new sensing controller for marine pollutant monitoring using field effect devices

MASTER IN MICRO AND NANOTECHNOLOGIES ENGINEERING

NOVA University Lisbon

September, 2024

DEPARTAMENT OF
MATERIALS SCIENCE

Integration of a new sensing controller for marine pollutant monitoring using field effect devices

CAROLINA DOS SANTOS PARREIRA

BSc in Micro and Nanotechnologies Engineering

Adviser: Dr. Bruno Veigas
Post-Doc Researcher, NOVA University Lisbon
Co-advisers: Dr. Joana Pinto
Assistant Professor, NOVA University Lisbon

Examination Committee:

Chair: Dr. Pedro Barquinha,
Associate Professor, NOVA University Lisbon
Rapporteur: Dr. Rita Branquinho,
Associate Professor, NOVA University Lisbon
Adviser: Dr. Bruno Veigas,
Post-doc Researcher, NOVA University Lisbon

MASTER IN MICRO AND NANOTECHNOLOGIES ENGINEERING

NOVA University Lisbon
September, 2024

Integration of a new sensing controller for marine pollutant monitoring using field effect devices

This document was created with Microsoft Word text processor and the NOVAthesis Word template.

ACKNOWLEDGEMENTS

Para a concretização e finalização deste meu percurso académico, pude contar com a ajuda de diversas pessoas sem as quais tal não teria sido possível. A todas elas, quero deixar por escrito um agradecimento especial.

Primeiramente, gostaria de agradecer à instituição que permitiu a realização deste projeto, a Faculdade de Ciências e Tecnologia da Universidade Nova de Lisboa, em especial ao Departamento de Ciência dos Materiais e CENIMAT|l3N, não só, por proporcionar aos seus alunos uma experiência no mundo da investigação, mas também pelas experiências académicas ao longo destes anos.

Também gostaria de deixar um especial agradecimento ao Professor Rodrigo Martins e à Professora Elvira Fortunato por tornarem possível a existência deste curso tão inovador que é o curso de Engenharia de Micro e Nanotecnologias e por todas as condições que permitiram esta experiência no CENIMAT|I3N.

I want to express my gratitude to everyone involved in the project SeaSenseX (MACAU/0022019) for allowing me to collaborate through this thesis. Working on something that can potentially contribute to positive change in the world is incredibly meaningful to me. Engineering is all about this: using knowledge and skills to make a real difference and improve the world around us. Thank you for the opportunity to be part of something impactful.

Aos meus orientadores Dr. Bruno Veigas e Dra. Joana Pinto, com quem tive o privilégio de trabalhar, agradeço por toda a disponibilidade, apoio e orientação prestada, sempre fazendo o possível para o meu sucesso. À Prof. Joana Pinto, tenho também a agradecer em especial por ter sido das melhores professoras que tive durante este percurso académico, pela inteligência e paciência com os seus alunos, ajudando sempre que preciso e fomentando o meu interesse por esta área. À Ana Santa, obrigado por toda a disponibilidade e paciência de santa para fabricar os sensores, sem si não teria sido possível.

Aos meus colegas de trabalho neste projeto Rui Azevedo e Rafael Snow, agradeço por terem partilhado esta experiência comigo e por estarem sempre prontos a ajudar em qualquer situação.

Agradeço também à Raquel Martins por se mostrar sempre disponível para me ajudar em qualquer situação desde o meu projeto de licenciatura.

A todos os meus amigos, e em especial ao Bando dos 4, Marianita, Joca e Ricardela, que me acompanham desde o início, e estão sempre disponíveis para me apoiar, seja academicamente ou na vida em geral, proporcionando a concretização dos meus sonhos e trazendo à tona o melhor de mim. Ao meu namorado Davi, agradeço toda a paciência ao longo destes anos, que venham muitos mais, até sermos velhinhos.

Um agradecimento muito especial à minha família, Mãe, Pai, Vó e Madrinha, obrigada por me permitirem concretizar os meus sonhos e me amarem como amam.

This work was financed by national funds from FCT - Fundação para a Ciência e a Tecnologia, I.P., in the scope of the projects LA/P/0037/2020, UIDP/50025/2020 and UIDB/50025/2020 of the Associate Laboratory Institute of Nanostructures, Nanomodelling and Nanofabrication – i3N.

“Our virtues and our failures are inseparable, like force and matter.
When they separate, man is no more.” (Nikola Tesla)

ABSTRACT

The preservation of the oceans is an urgent global issue driven by increasing pollution in marine ecosystems, which negatively impacts marine life and leads to long-term ecological damage. To mitigate these effects, it is essential to develop innovative technologies that can monitor pollutants, particularly heavy metals, with greater accuracy and accessibility, overcoming the limitations of current solutions.

This work is part of the SeaSenseX project and aims to develop a portable device equipped with sensors based on the CMISFET (Charge-Modulated-Ion-Sensing-Field-Effect-Transistor) architecture. This device utilizes a control electrode and a sensitive area to modulate the channel of an integrated MOS (Metal-Oxide-Semiconductor) transistor. The sensors are fabricated on flexible PEN substrates at CENIMAT|I3N and were tested using two methodologies: i) an existing semiconductor parameter analyzer in the laboratory, and ii) a PCB (Printed Circuit Board) connected to an Arduino for real-time data acquisition. Two types of MOSFETs, a commercial (CD4007UB) and one especially developed for this project (MKProt), were compared in measurements conducted with pH buffer solutions.

Moreover, a microfluidic system was developed and tested to optimize the sensitivity of the sensors. This improvement allowed for this technology to go from a reported sensitivity of 39 ± 1 mV/pH to 54 ± 1 mV/pH, close to the theoretical maximum of approximately 59 mV/pH unit. The MKProt MOSFET, which demonstrated significant advantages in data acquisition, was utilized for measurements with mercury chloride and cadmium chloride solutions. The device successfully detected mercury concentrations ranging from 1 ppm to 15 ppm and cadmium concentrations between 1000 ppm and 3000 ppm. The recorded sensitivities for detecting these metals are 0.11 ± 0.01 mV/Log(ppm) for mercury and 0.41 ± 0.01 mV/ppm for cadmium, respectively.

In addition, preliminary analyses were performed using membranes impregnated with silver nanoparticles (Ag-NPs) deposited on Nafion on the sensor surface. These analyses aimed to explore options for optimizing heavy metal detection. However, further research is necessary to assess the impact of these modifications and ensure the reliability and performance of the sensors in real-world applications.

Keywords: Heavy metals; CMISFET; flexible substrate; microfluidics system; Nafion; Ag-NPs membrane.

RESUMO

A preservação dos oceanos é uma questão global urgente devido ao aumento da poluição nos ecossistemas marinhos, que afeta a vida marinha e causa danos ecológicos a longo prazo. Para mitigar esses impactos, é essencial desenvolver tecnologias inovadoras para monitorar poluentes, como metais pesados, de forma mais precisa e acessível, superando as limitações das soluções atuais.

Este trabalho, parte do projeto SeaSenseX, visa desenvolver um dispositivo portátil com sensores baseados na arquitetura CMISFET (*Charge-Modulated-Ion-Sensing-Field-Effect-Transistor*), utilizando um elétrodo de controlo e uma área sensível para modular o canal de um transístor MOS (*Metal-Oxide-Semiconductor*) integrado. Esses sensores, fabricados em substratos flexíveis de PEN no CENIMAT|I3N, foram testados usando duas metodologias: i) um analisador de parâmetros de semicondutores existente em laboratório e ii) uma PCB (*Printed Circuit Board*) acoplada a um Arduino para aquisição de dados em tempo real. Dois MOSFETs, um comercial (CD4007UB) e um especialmente desenvolvido para este projeto (MKProt), foram comparados nas medições realizadas com soluções buffer de pH.

Além disso, foi desenvolvido e testado um sistema de microfluídica de forma a otimizar a sensibilidade dos sensores. Esta melhoria permitiu que a sensibilidade dessa tecnologia passasse de um valor de 39 ± 1 mV/pH para 54 ± 1 mV/pH, aproximando-se do máximo teórico de aproximadamente 59 mV/pH. O MOSFET MKProt, que demonstrou vantagens na aquisição de dados, foi utilizado nas medições com soluções de cloreto de mercúrio e cloreto de cádmio. A eficácia na deteção de metais pesados foi comprovada, detetando concentrações de mercúrio de 1 ppm a 15 ppm e de cádmio de 1000 ppm a 3000 ppm. As sensibilidades registadas para a deteção desses metais foram de 0.11 ± 0.01 mV/Log(ppm) e 0,41 ± 0,01 mV/ppm, respetivamente.

Foram realizadas ainda análises preliminares com membranas impregnadas com nanopartículas de prata depositadas sobre Nafion na superfície do sensor, de forma a procurar opções para a otimização na deteção de metais pesados. Mais pesquisas são necessárias para avaliar o impacto dessas modificações e garantir a confiabilidade e o desempenho dos sensores em aplicações do mundo real.

Palavas chave: Metais pesados; CMISFET; substratos flexíveis; sistema de micrifluídica; Nafion; membranas Ag-NPs

CONTENTS

LIST OF FIGURES

LIST OF TABLES

ACRONYMS

ADC	Analog-to-digital converter
CENIMAT	Centro de Investigação de Materiais
CMFET	Charge-modulated field-effect transistor
CMISFET	Charge-modulated ion-sensitive field-effect transistor
CMOS	Complementary metal-oxide-semiconductor
CVD	Chemical vapour deposition
EIS	Electrolyte-insulator-semiconductor
FED	Field-effect device
FET	Field-effect transistor
IC	Integrated circuit
ISFET	Ion-sensitive field-effect transistor
LOD	Limit of Detection
LPCVD	Low-power chemical vapour deposition
MIS	Metal-insulator-semiconductor
MOSFET	Metal-oxide-semiconductor field-effect transistor
PCB	Printed Circuit Board
PEN	Polyethylene naphthalate
PECVD	Plasma-enhanced chemical vapour deposition
PVD	Physical vapour deposition
RT	Real-time
SNR	Signal-to-noise ratio
SMU	Source measure unit
SPA	Semiconductor Parameter Analyzer
TC	Transfer Curves
UN	United Nations
VS	Voltage Sweeps

SYMBOLS

C	Capacitance
D	Dissipation factor
I_{D}	Drain Current
I_{DS}	Drain-to-Source Current
I_{off}	Off Current
I_{on}	On Current
I_{REF}	Reference current
pHpzc	Point of zero charge
V_{ADC}	Circuit output voltage inserted in the ADC
V_{CG}	Control-gate voltage
V_{D}	Drain Voltage
V_{G}	Gate Voltage
V_{REF}	Reference Voltage
V_{TH}	Threshold voltage
μ	Electrical Mobility

1

MOTIVATION AND OBJECTIVES

The preservation of oceans has become a crucial global issue due to the escalating pollution caused by the unchecked disposal of thousands of chemical substances into marine ecosystems. This pollution severely impacts all forms of marine life, leading to long-term ecological damage. In response to this growing concern, Global Goal 14 of the UN's 2030 Agenda focuses on conserving and sustainably using oceans, seas, and marine resources. [1] Achieving this goal requires immediate action to develop innovative monitoring technologies that can detect and manage marine pollutants with greater accuracy, reproducibility, and affordability than existing solutions. These technologies are vital to overcoming the limitations of current monitoring methods and ensuring the long-term health and sustainability of marine ecosystems.

According to the World Health Organization, millions of people are estimated to die each year due to poisoning or exposure to heavy metals through contaminated food, leading to severe health issues. Pollutants, such as heavy metals, enter marine ecosystems through various sources, including wastewater from industrial and agricultural activities, oil spills, and the use of pesticides and fertilizers. As a result, approximately 300 million tons of heavy metals are released into natural water bodies annually, causing significant environmental damage and posing risks to both marine life and human health. [2]

Heavy metals such as arsenic, cadmium, chromium, lead, and mercury are highly toxic and are classified as significant public health concerns and human carcinogens. These metals can bioaccumulate in biological systems, meaning they build up in organisms over time, potentially leading to dangerous concentrations. Even at relatively low exposure levels, these toxic metals are recognized as systemic toxicants, capable of causing damage to multiple organs, leading to serious long-term health effects. Their persistent presence in ecosystems, especially marine environments, amplifies the risks to both human health and wildlife. [3]

Therefore, it is imperative to develop effective research methods and advanced detection technologies for these pollutants. Accurate and reliable monitoring is crucial to assess contamination levels, mitigate risks, and prevent further harm to both ecosystems and human health. By identifying the presence of heavy metals early on, targeted interventions can be implemented to reduce their impact, ensuring safer environments and contributing to the sustainable use of marine resources.

The primary objective of this project is to develop and optimize a portable device equipped with sensors based on a Charge Modulated Ion Sensitive FET (CMISFET) architecture. These sensors will be integrated onto flexible substrates (PEN) to enable the detection and quantification of various heavy metals in water using electrochemical sensing methods and a microfluidics-based approach. This initiative is part of the Sea-SenseX project, titled "Next-generation microsensors for marine mutagens and carcinogens", a collaboration between CENIMAT, I3N research units, and the University of Macao.

This hybrid approach will strike a balance between cost efficiency and sensor flexibility while achieving high accuracy in detecting potential mutagens and carcinogens in marine environments.

This work was financed by national funds from FCT - Fundação para a Ciência e a Tecnologia, I.P., in the scope of the projects LA/P/0037/2020, UIDP/50025/2020 and UIDB/50025/2020 of the Associate

Laboratory Institute of Nanostructures, Nanomodelling and Nanofabrication – i3N), as well as through the projects MACAU/0002/2019 (SeaSenseX).

2

INTRODUCTION

Marine pollution is an escalating problem in today's world. Similar to other micropollutants, including pharmaceuticals, cosmetics, pesticides, and industrial or household chemicals, heavy metals are becoming an increasingly significant environmental concern. [4]

Heavy metals are a group of metals and metalloids that have relatively high densities and are toxic or poisonous at low concentrations, being very detrimental to the health of all living organisms. These materials can be produced and enter the environment through biogeochemical processes, however, the main source of these metals in the marine ecosystem is through industrial processes, mining, agricultural runoff, and improper waste disposal. Once they are in the environment, they can accumulate in the soil, water, and living organisms, leading to long-term ecological issues, once they are not biodegradable, and various health problems. [5] There are over 50 elements classified as heavy metals, encompassing transition metals, some metalloids, lanthanides, and actinides. While some metals are essential for cellular functions such as iron, copper and zinc, others, such as cadmium or mercury, have no known physiological function in eukaryotes and are purely toxic.[6] Some of the most common heavy metals include mercury, cadmium, arsenic and lead. The maximum permissible values in drinking water for these trace metals in ppm units, according to World Health Organization's Drinking Water Guidelines (WHO) from 2011, are registered in the following Table 2.1. [7]

Table 2.1:Permissive Limits in drinking water according to WHO's Guidelines. [7]

Heavy Metal Ions	**Hg**	**Cd**	**As**	**Pb**
WHO's Permissive Limit (ppm)	0.001	0.003	0.1	0.001

Therefore, the development of new monitoring technologies for marine pollutants is essential, ensuring accuracy, reproducibility, and affordability beyond the limitations of current state-of-the-art solutions. SeasenseX addresses these challenges as primary goals, aiming to design a device that is not only highly accurate and reliable but also portable and accessible to all users.

Heavy metal trace detection is primarily conducted by expensive methods like spectroscopic techniques, such as atomic absorption spectroscopy (AAS), inductively coupled plasma mass spectroscopy (ICP-MS), X-ray fluorescence, and neutron activation analysis. These techniques are very effective and detect a wide range of elements demonstrating a high sensitivity and very low detection limits (femtomolar range), however, these methods are very costly, as they require expensive equipment and highly trained operators to perform the preparation and analysis of the samples and have long detection time, only being suitable for on-laboratory analysis. [8], [9]

Therefore, portability and easy adaptability for in situ measurement, low cost, and high integration of detection systems are crucial directions for the advancement of heavy metal ion sensing technologies. To address these challenges, electrochemical techniques emerge as a promising point-of-care testing method, due to the various advantages like low-cost production, small size, simple equipment, reliability and faster detection time, offering also the possibility of heavy metal detection in-situ, without the need for sample transportation.

Recently, electrochemical sensors (ECS) have garnered significant attention for the detection of heavy metals in various fields such as food, agricultural products, medicine, environment, and health, due to their ability to interface with sensing electrodes modified with specific materials or bio sensitive elements to enhance sensitivity and detection limits. [10] Among the several types of electrochemical sensors are the Field-

Effect Devices (FEDs) which have demonstrated several advantages and have gained significant interest in recent years for biological sensing applications. In particular, the field effect transistor (FET), as a novel electronic sensing technique, shows great promise for the rapid and effective detection of chemicals and biomolecules. Compared to other analytical techniques, FET sensors offer several advantages, such as fast response times, ease of operation, low-cost mass production, relatively low noise, and high sensitivity. The sensing channel material is the core component of FET devices, as it directly impacts the overall sensing performance, due to the interaction between the analyte and the channel material that induces the change of carriers in the channel.

Notably, FET sensing platforms have shown significant potential for the rapid detection and monitoring of heavy metal ions. Several FET sensors have been developed for the analysis of heavy metals. [9]

2.1 Field Effect Sensing Devices

In recent years, among the new generation of biosensing platforms, field effect devices (FED) for biological detection have become a basic structural element. [11] These devices are usually used as the transducer and their structure is based on the architecture of a metal-insulator-semiconductor (MIS) capacitor or metal-oxide-semiconductor (MOSFET). These designs undergo slight modifications to address the challenges and requirements of integrating biological reactions with electronic devices. FED sensors enable real-time monitoring of biomarkers without requiring labelling or reporter molecules. FEDs can detect minute molecular interactions at the surface, which influence the charge distribution in the transistor channel, thereby modulating the electrical signal output. [12]

The structure and operation principles of electrolyte-insulator-semiconductor (EIS) capacitors and ion-sensitive field effect transistors (ISFET) are presented in the next sections.

2.1.1 Electrolyte-Insulator-Semiconductor (EIS)

The Metal-Insulator-Semiconductor (MIS) capacitor is one of the most useful devices in the study of electronic circuits with a simple structure, incorporating a semiconductor insulator interface between two electrodes, with a variable capacitance, which serves as a model for the development of a sensitive layer. [13]

The electrolyte-insulator-semiconductor (EIS) capacitor is one of the modified structures for biosensing, as mentioned before. This structure emerged from MIS capacitor where the gate electrode is replaced by an electrolyte and a reference electrode, and the insulator layer (oxide) is in direct contact with the electrolyte, therefore, modulation of the device's response is accomplished by changes in the solution, that affects the oxide's surface potential.[13] ,[14]

The following image (Figure 2.1) represents a schematic comparing the structure of a MIS and EIS. [14]

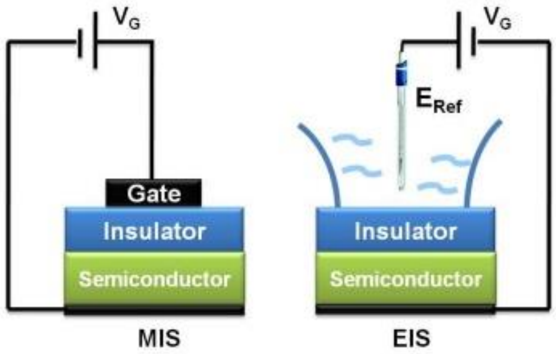

Figure 2.1: Schematic illustration of MIS and EIS structures. [14]

2.1.2 Ion-Sensing-Field-Effect-Transistor (ISFET)

Analogous to what occurs with the EIS sensor referred to earlier, the Ion-Sensing-Field-Effect-Transistor (ISFET) sensor has a structure and operation similar to a Field-Effect-Transistor (MOSFET). Similarly, the gate electrode is replaced by an electrolyte and a reference electrode, leaving the gate directly in contact with the electrolyte. [13]

A schematic comparing the structure of a FET and an ISFET is represented in Figure 2.2. [14]

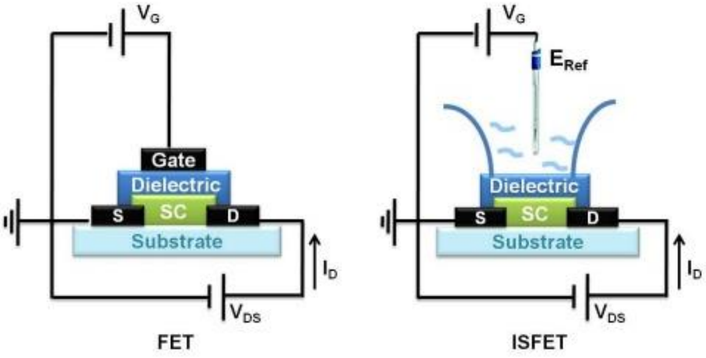

Figure 2.2: Schematic illustration of FET and ISFET structures. [14]

Currently, within the extensive range of FET sensors, the ISFET emerges as one of the most widely recognized categories of electrical biosensors. [15]

ISFET-based sensors offer numerous advantages, particularly in applications related to pH sensing and ion concentration measurements. However, they come with certain inherent drawbacks that can limit their use in specific applications related to device stability, such as drift and hysteresis. [16]

Drift in ISFET-based sensors is defined by threshold voltage instability over time. This can result in a gradual shift in the measured output, even when the conditions of the sample remain constant. Drift can be a significant issue in applications that require high precision and long-term stability. [17]

Hysteresis is a memory effect observed in these devices, where the response depends on its prior history of exposure to samples. This means that the sensor's output may differ when measuring a sample with a particular pH after it has been exposed to a different pH value, even if the sample returns to its original pH. hysteresis can hinder accurate and reproducible measurements. [18]

Despite these challenges, ISFET-based sensors remain valuable tools in various applications, particularly where their advantages, such as small size, compatibility with microelectronics, and sensitivity to specific ions, outweigh the drawbacks.

However, researchers continue to work on improving these devices to extend their use to even more demanding applications and considerable efforts have been made to develop better architectures. [19]

2.2 Charge-Modulated-Ion-Sensing-Field-Effect-Transistor (CMISFET) Sensor

As seen previously, the ISFET and EIS sensor, based on the field-effect structure, has only one structural modification, which is the replacement of the transistor/electrode gate contact by an electrolyte and a reference electrode. These architectures hold great significance in the field of sensors. However, the sensor structure can present several issues due to the poor conditioning of the device and the electrolyte solution, posing a significant obstacle to device miniaturization.

Consequently, to overcome the challenges posed by these devices, extensive research has been conducted towards ISFET-based structures that do not require an external reference electrode, potentially incorporating it on-chip within the device. An example of such accomplishment is the charge-modulated FET architecture (CMFET), introduced by Barbaro et al in 2006. [20] This proposed device is based on the floating-gate MOS transistor with a control--gate that acts as the reference electrode and a sensitive area activated by charge induction, as shown in the following Figure 2.3. [20]

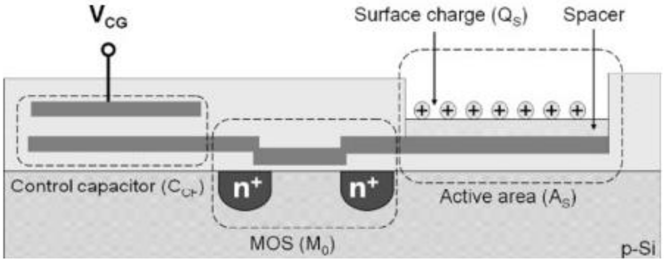

Figure 2.3: Illustration of the proposed CMFET in [20].

Considering the concept mentioned earlier, an innovative structure has been developed by Veigas et al. The device consists of a flexible and disposable sensing electrode integrated with a commercial MOSFET. Because the transistor is activated through control-gate capacitive coupling to a floating gate, it operates independently of the materials and intrinsic characteristics of the transistor. Additionally, the sensor and its sensitive area are physically separated from the transducer (MOSFET), which is encapsulated and integrated into the backend electronics without needing a reference electrode. [21] This allows a separation between the wet and the dry area where the transistor is activated, as shown in the following Figure 2.4. [22]

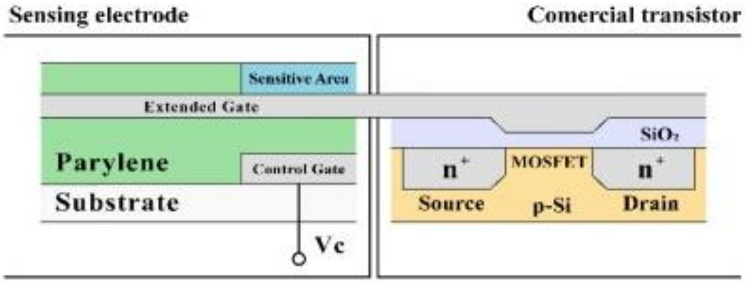

Figure 2.4: Illustration of the proposed CMISFET in [21]. [22]

This method enables higher stability and a longer lifetime of the device while simultaneously reducing the complexity and production cost of the disposable sensing electrode. An important aspect that distinguishes CMISFETs from ISFETs and EIS sensors is the reference electrode. In ISFETs and EIS systems, the reference electrode is typically non-miniaturizable. This electrode, aside from being bulky, complicates the experimental setup, making integration into portable or miniaturized systems more difficult and limiting its use in compact environments or wearable devices. Another key consideration for CMISFETs is ensuring that the transistor is impermeable to the test solution, allowing sensitivity to be maintained without compromising the structural integrity of the sensor. This is particularly important to ensure reliable measurements and sensor durability in real-world operating conditions, especially when exposed to corrosive or conductive solutions, such as in pH testing or heavy metal detection. By eliminating the need for a traditional reference electrode and ensuring the device's impermeability, CMISFETs offer a significant advantage in terms of miniaturization and versatility for portable and field applications. [21]

The variation in potential detected by the CMISFET is a result of the interaction between the sensitive layer and a test sample, as in previous methods, which will generate charged ions and consequently induce the change of carriers in the material. This interaction results in alterations in the transistor's characteristic curves, such as mobility (μ), threshold voltage (V_{th}), on/off ratio (I_{on}/I_{off}) and source-drain currents (I_{ds}), where the chemical information is converted into an electrical signal that can be easily measured and processed. [15]

This makes CMISFET an ideal choice for applications requiring high sensitivity and accuracy in the detection of various chemical species. It also provides real-time and non-destructive measurements, as well as compact size, low power consumption and compatibility with microfabrication processes.

This design can be used in devices adequate to detect pollutants present in marine environments, such as heavy metals and polycyclic aromatic hydrocarbons (PAHs). These elements are responsible for increasing oxidative DNA damage and preventing DNA repair. [23]

FET biosensors in general have been successfully used for the sensitive detection of proteins, glucose, DNA, and cells, illustrating the rapid development of this exciting research field and wide range of applications.

Field effect devices (FEDs), despite their many advantages, face certain challenges related to device stability and reproducibility. For applications where low-cost disposable sensors are preferred, these issues could be resolved, though this approach introduces new challenges. In particular, the use of low-cost flexible substrates, such as plastic and paper, to produce field effect sensors would require low-temperature fabrication processes to ensure compatibility with these materials.

The sensitivity of the sensor is primarily influenced by the intrinsic properties of the sensitive layer and the ionic concentration, which is associated with the Debye length. [24] This parameter links the proximity of ions to the surface with the surface potential. As ions approach the sensitive layer, the surface potential increases, reaching its peak when ionic bonds are formed.

The sensitivity of FET sensor to pH buffer solutions is usually described by the ion-site binding model, which describes how protons (H^+) or other ions from the solution interact with specific binding sites on the sensitive layer, and Nernst's law, which predicts a theoretical limit of 59.2 mV/pH at 298 K. This theoretical value represents an ideal scenario of a sensitive oxide; actual sensors may exhibit slightly different sensitivities due to factors like sensor design, ionic strength, temperature variations, and the presence of competing ions. [25]

2.3 Optimization of the Sensitive layer

Nanomaterials exhibit distinct properties, such as superior electrochemical characteristics, substantial surface area, and adjustable electrical conductivity, making them highly suitable for sensing applications, especially in electrochemical sensing. [26]

Recently, the incorporation of nanomaterials into electrochemical sensor platforms has become a potent analytical approach for detecting heavy metals. The effectiveness of electrochemical sensing platforms can be greatly improved by chemically modifying bare electrodes with efficient electron mediators. Thanks to their extensive surface area, adaptability for modifications, and remarkable quantum mechanical properties, nanomaterials are ideal candidates for this purpose. The use of nanomaterials is promoted because of their solid adsorption, high electron energy, and biocompatibility, which are appropriate for heavy-metal sensor applications. [27],[28]

A variety of nanomaterials, including carbon-based substances, metallic nanoparticles (NPs), and silicon-based materials, have been utilized to enhance electrode performance. The superior functionality of nanomaterial-based sensors is attributed to the nanoscale engineering of the electrode surface, which enhances catalytic activity, boosts conductivity, increases the active surface area, and speeds up electrode kinetics. [28]

Gold nanoparticles (Au-NPs) and silver nanoparticles (Ag-NPs) are among the most widely used nanomaterials due to their distinctive physicochemical properties at the nanoscale. They are favoured for their ease of preparation, straightforward fabrication process, and high chemical stability. The remarkable characteristics of nanoparticles (NPs), including adjustable physicochemical properties, enhanced stability, high electrical conductivity, catalytic activity, and a large surface area, have garnered significant interest in their application for electrochemical sensors aimed at detecting heavy metal ions. [29],[27]

Modifying an electrode with NPs can provide multiple benefits, such as the elimination of memory effects and interferences from coexisting ions, lowering the limit of detection (LOD) for heavy metal detection., showing high sensitivity and selectivity for detection. [30]

One of the many advantages of this sensor technology is its ability to modify the sensing layer according to specific needs and objectives, owing to its simple structure. In this work, a preliminary analysis was conducted on the sensor's response when membranes containing silver nanoparticles (Ag-NPs) were deposited on the surface of the sensitive layer. These nanoparticles, provided by Brazilian researchers, were deposited using Nafion as the adhesion promoter. Nafion is a sulfonated tetrafluoroethylene-based fluoropolymer–copolymer with conductive properties. As a cation exchange polymer, Nafion helps block anionic species from reaching the electrode surface while allowing cation conduction to pass through, thus leading to improved selectivity. [31],[32]

2.4 CMISFET Sensor Controller

As previously mentioned, one of the primary objectives of this work is to create a sensor capable of reliably detecting heavy metals, while also designing a completely portable device that enables on-site testing without the need for laboratory-based equipment and is accessible to all users. To achieve this, a software made in Python was developed by another master’s student to mimic the testing made in laboratory [33]. This software facilitates the interaction of all the necessary hardware components, including the CMISFET sensor, the PCB (developed by a Master’s Student (2023) [33] in collaboration with the University of Macao), and the Arduino. The software simplifies data acquisition from raw data acquired by the Arduino, enhancing the usability of the device for real-world applications, and enabling a Lab-on-chip device. This PCB was designed to accommodate both the commercial MOSFET CD4007UB or the custom-made MOSFET (MKProt), which was developed by researchers at the University of Macao, playing a key role in enhancing the sensor's performance and adaptability for detecting heavy metals.

In this monitoring device, the designed PCB serves as the interface between the CMISFET sensor and the Arduino microcontroller, enabling reliable on-site measurements without compromising sensor performance. The system allows for the precise adjustment of voltage, facilitating a wide range of analyses through the CMISFET sensor. The sensor’s response is processed through the custom MOSFET (MKProt), which generates a variable drain current. This current is then filtered to remove unwanted noise, ensuring a clear signal.

After filtering, the current is amplified and converted into voltage, a key step that enables the Arduino to accurately interpret the data. This voltage conversion is critical for ensuring accurate data acquisition and processing, allowing for the detection and analysis of small variations in current and voltage on the surface potential. This process is comparable to laboratory-grade equipment like the Agilent system, enabling precise detection and interpretation of subtle changes in the sensor's response, ensuring high-quality results in practical applications. [34]

3

MATERIALS AND METHODS

. The following chapter first briefly presents the fabrication method of the sensors produced. Next, it describes the solutions used for testing the sensors, as well as the testing methods on two different platforms. Finally, Ag-NP membranes are analyzed based on their structure.

3.1 Sensor's Fabrication

The proposed CMISFET sensor consists of four sequentially deposited layers on a PEN substrate. The substrate is heat-treated at 150°C, cleaned with ultrasonic baths in acetone and isopropyl alcohol, and dried. The sensor layers include molybdenum top and bottom contacts (60 nm thick, deposited by RF sputtering), a Parylene-C dielectric layer was deposited in two subsequent depositions of 0.3 g (~400 nm, deposited via CVD), and a tantalum oxide (Ta_2O_5) sensitive layer (~100 nm, deposited by RF sputtering). More details about the deposition of each layer can be found in Appendix A.1, along with a descriptive image of each layer. Each layer is carefully deposited and patterned by aligning a physical mask (Appendix A.2), ensuring uniformity and reproducibility through specific deposition conditions. Images of the sensor batches produced on PEN substrate can be found in Appendix A.3.

3.2 pH and Heavy Metal Testing Solutions

For the tests conducted to observe the sensor's response to pH differences, the sensitive was exposed area to constant ionic strength buffer solutions (4, 7 and 10 with a precision of ± 0.01 (HANNA instruments)).

For the heavy metal detection, solutions of 3000 ppm of two different heavy metals, namely mercury (II) chloride 99% ($HgCl_2$, CAS No 7487-94-7, Sigma-Aldrich) and cadmium chloride hydrate 98% (CdCl2.xH2O, CAS No 654054-66-7, Sigma-Aldrich), were initially prepared using distilled water in flasks of 50 mL and stirred at room temperature for around 1 hour at a velocity of 430 rpm to guarantee the complete dissolution of the particles. These solutions were subsequently diluted to lower concentrations in flasks of 10 mL to match the sensitivity of the sensors for each heavy metal. Solutions with concentrations between 1 ppm and 25 ppm were evaluated for Hg and 1000 ppm and 300 ppm for Cd ions. To preserve the initial properties of the solutions, these were maintained in a dark, dry, and cool place.

3.3 Electrical Characterization of CMISFET Sensor

For the electrical characterization of the sensors, two different software tools were utilized. Initially, an Agilent 4155C semiconductor parameter analyzer (SPA), paired with a test fixture 16442A, was used alongside the Keysight Easy EXPERT group+ software. Subsequently, a developed Controller board was employed. This tool was developed as part of the efforts to create the main portable device.

To facilitate and ensure effective sensor measurements in both approaches, an encapsulated electrical connector with integrated pogo pins was designed. This connector was developed using 3D modelling by another master's student (Rafael Neves), enabling easier and more reliable sensor connections.

3.3.1 Characterization in Agilent 4155 C SPA

To perform the principal electrical characterization of the sensors it was used the Agilent 4155 C SPA and test fixture 16442A. A MOSFET CD4007UB was used to compare the initial results with the custom-made MOSFET (MKProt) made in collaboration with the University of Macau.

The CMISFET sensors were evaluated using two different testing methodologies at room temperature (≈25ºC), which were similar for both MOSFETs tested. Firstly, it was performed an analysis of the transfer characteristic curves, with the sensor CMISFET operating in the saturation regime (V_{DS} = 0.5 V) and maintaining the V_{CG} sweep between 0.8 V and 2 V. And finally, it was analyzed the response of the sensor in real-time monitoring the drain current and keeping the values of voltage in the gate and the drain constant. For all solutions and methodologies, a dry test was performed on the sensor testing the transfer curve of the sensor without any solution, to check if the signal of the bottom electrode was transferred to the MOSFET gate.

3.3.1.1 Analysis of pH solutions

First, 50 µL of pH 10 buffer solution is pipetted onto the sensitive area of all sensors, maintaining it for 10 to 30 minutes for the sensing platform to stabilize, before every measure cycle, not allowing the sensor to dry out. To extract the transfer curve characteristics through the voltage sweeps, it was made several measurements with the pH 10 buffer, until it registered no significant shift (≤ 0.5 µA for CD4007B MOSFET and ≤ 0.05 mA for MKProt MOSFET), once the sensing response stabilized, it was performed an exchange of pH solution to pH 7, removing the previous solution without touching the sensor and pipetting the same quantity of the new pH solution (using a different tip). This process was repeated to complete the cycle of pH10 → pH7 → pH4 repeating it 2 times to have statistically significant variability.

A similar procedure was employed for the continuous real-time monitoring of the drain current, involving a full cycle of pH solutions in contact with the sensor (10 → 7 → 4 → 7 → 10). This cycle was also repeated twice, and each pH buffer solution was left for approximately 300 seconds until the data showed no significant variation, ensuring accurate and consistent readings.

The influence of the amount and regularity of solution deposition was also studied through a microfluidic system, where the deposition rate per minute was controlled using the same kind of electrical connector but adapted to the microfluidics tests. For this experiment, a 10 mL syringe was attached to a Legato 210 syringe pump. The pump withdrew the solution through a microfluidic tube at a 200 µL/min rate, allowing the solution to flow over the sensor. The measurement cycles were conducted similarly to the previous ones, with the only difference being the switching of flasks containing different buffer solutions.

3.3.1.2 Analysis of heavy metals solutions (Mercury and Cadmium)

Using a similar method of analysis, the sensors were also tested exposing the sensitive area to solutions of two different heavy metals (mercury (II) chloride 99% and cadmium chloride hydrate 98%). For these solutions, it was also tested the transfer curves characteristics and the continuous real-time. Initially, 50 µL of distilled water is pipetted onto the sensor's surface. The distilled water is left for around 10 minutes, until the response of the sensor is stabilized, and analogous to the previous analysis, it is performed an exchange of solutions, pipetting a solution of mercury or cadmium of a specific concentration. The solution exchanges are carried out by gradually increasing the concentration of the deposited solutions. For real-time monitoring analysis, a cyclic approach was used, progressively lowering the concentrations of the buffer solutions to test the sensor's ability to partially regenerate its signal.

3.3.1.3 Optimization of the Sensitive Layer

To enhance the sensitivity and selectivity for heavy metal detection, membranes containing silver nanoparticles were applied to the sensor's surface for a preliminary analysis. These membranes were adhered using Nafion perfluorinated resin solution (CAS 31175-20-9, Sigma-Aldrich), which was deposited between the sensor surface and the nanoparticle membranes.

Initially, an analysis was conducted on sensors with only Nafion deposited to evaluate whether this modification offered any advantages to the sensing behaviour. This assessment was crucial to establish the optimal quantity of Nafion required for effective adhesion and functionality on the sensor surface. By understanding the baseline performance of Nafion alone, the subsequent analyses with silver nanoparticles could be more accurately interpreted, ensuring that any observed enhancements in sensitivity and selectivity could be directly attributed to the incorporation of silver nanoparticles.

3.3.2 Characterization using CMISFET Controller Board

One of the primary goals of the SeasenseX project is to ensure that the designed device is user-friendly and accessible for all users, eliminating the dependence of on-laboratory-based tests without compromising the reliability of the results. For this, a custom controller board was designed, in the context of a previous master's thesis and collaboration with an investigator in this project, that enables data collection and visualization directly on-site, through the integration of essential components, such as a Printed Circuit Board (PCB) developed especially for this project in collaboration with the University of Macao and the CMISFET sensor connected to the PCB through an Arduino microcontroller (Appendix A.4) [33]. This PCB was designed to accommodate the custom-made MOSFET (MKProt), which was developed by researchers at the University of Macao. This custom component plays a key role in enhancing the sensor's performance and adaptability for detecting heavy metals.

The analyses performed in this software are analogous to those previously mentioned, also analyzing the behaviour of voltage sweeps as well as real-time behaviour. For the voltage sweeps it’s necessary to define parameters like initial and final V_{CG} voltages (control gate voltage), V_D voltage (drain voltage), number of voltage steps and number of points to acquire per step, controlling the V_{ADC} voltage. For continuous real-time monitoring is necessary to define the V_{CG} voltage, which is extracted from an analysis of the voltage sweeps and define a V_D value. The result of this analysis will reflect the variation in the V_{CG} value over real-time.

3.4 Structural Characterization of Ag-Nps Membranes

To characterize the morphology of the membranes and elemental analysis, two samples, each with different concentrations of Ag-NPs, were visualized using Scanning Electron Microscopy (SEM) analysis and Energy Dispersive X-Ray Spectroscopy (EDS**.** This characterization allowed for a detailed examination of the distribution, size, and overall structural properties of what composed the membranes, providing insights into how these factors may influence the sensor's performance in heavy metal detection.

4

RESULTS AND DISCUSSION

This chapter presents the analysis of the obtained results for CMISFET sensors produced on PEN substrates, tested with both pH and heavy metal solutions. Initially, the electrical characterization results are presented, obtained using the Agilent 4155C SPA paired with a 16442A test fixture. Following this, a custom CMISFET controller board was employed to integrate the sensor, PCB, and Arduino for further testing and comparison. The results are processed to gather information on the sensitivity using various methodologies for both MOSFET and the detection limit of the sensor for each heavy metal. This chapter also details the optimization of the detection process, focusing on maximizing signal resolution and improving the signal-to-noise ratio (SNR).

4.1 Sensor Fabrication and Functionality Testing

The sensors fabricated at CENIMAT consist of four essential layers that are deposited using different methods onto flexible PEN substrates. These layers, in the order of deposition, include the bottom electrode made of molybdenum (Mo), a dielectric layer deposited in two successive layers of Parylene-C, the top electrode also made of molybdenum, and the sensitive layer composed of tantalum oxide (Ta_2O_5). The following Figure 4.1 illustrates this configuration in detail.

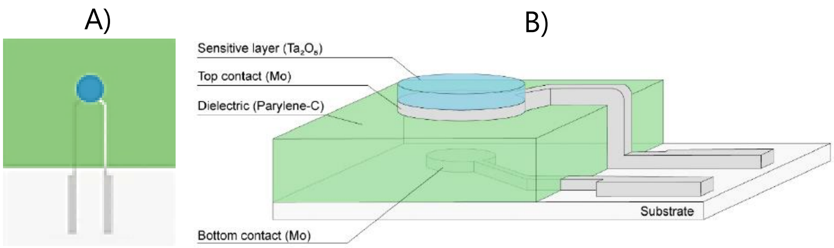

Figure 4.1: CMISFET sensor configuration with layer deposition: (A) Top view of the sensor. (B) Cross-section of the sensor.

Before the electrical characterization, a dry capacitance test was conducted using an LCR meter to verify the functionality of the sensors. This test was performed to confirm that the sensors operated within a capacitance (C) range of 0.100-0.400 nF, [19] as established in previous studies and if the dissipation (D) factor, which represents the energy loss in an oscillating circuit, was relatively low (around 0.045-0.065). These measurements can be found in Appendix A.5.

4.2 Electrical Characterization of CMISFET Sensors

The detection protocol directly influences the results in terms of signal quality and error. To address this, a comprehensive study was conducted on sensors fabricated on PEN substrates to develop an optimal detection and data analysis protocol. This protocol is essential for accurately comparing the results of sensors produced, ensuring consistency and reliability in the evaluation of their performance.

The CMISFET sensors were tested using an alternative connection topology where the bias voltage is applied to the top electrode and the connection to the MOSFET gate is in the bottom electrode, as shown in

Figure 4.2, since this alternative connection showed results with better sensitivity and faster responses, in previous studies, from a master student. [22]

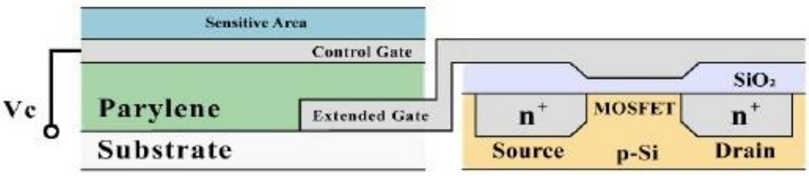

Figure 4.2: Connection schematic of CMISFET sensor: Proposed connection topology having the bottom electrode control gate connected to the MOSFET and applying voltage (VC) on the top extended gate electrode. [22]

4.2.1 Characterization of MOSFET Functionality

Since the sensor's analysis relied heavily on the transistor used as a transducer, it was developed in collaboration with researchers at the University of Macao a custom MOSFET tailored to the specific requirements of this project. This custom MOSFET, referred to as MKProt (shown in Figure 4.3.A), was designed to ensure optimal performance in the monitoring device. To evaluate the effectiveness of this newly developed component, comparisons were made with the commercially available MOSFET CD4007UB (shown in Figure 4.3.B), which had been used previously in sensor testing by another Master's student. [33]

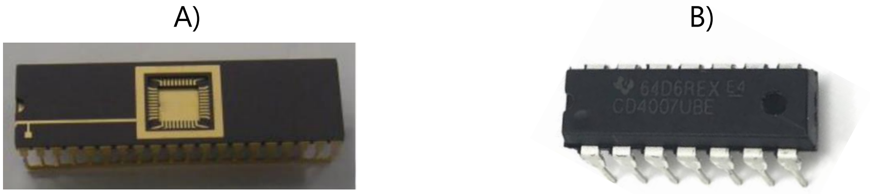

Figure 4.3: Used MOSFETs; A) Packaging of the developed MKProt; B) Commercial MOSFET CD4007UB by Texas Instruments

Firstly, a comparison between the two devices was conducted to assess how well the MKProt performed relative to the commercial MOSFET CD4007UB in meeting the project's goals. This analysis focused on the characteristics of the transfer curves of both MOSFETs.

The relationship between I_D and V_{CG} can be seen in the following images.

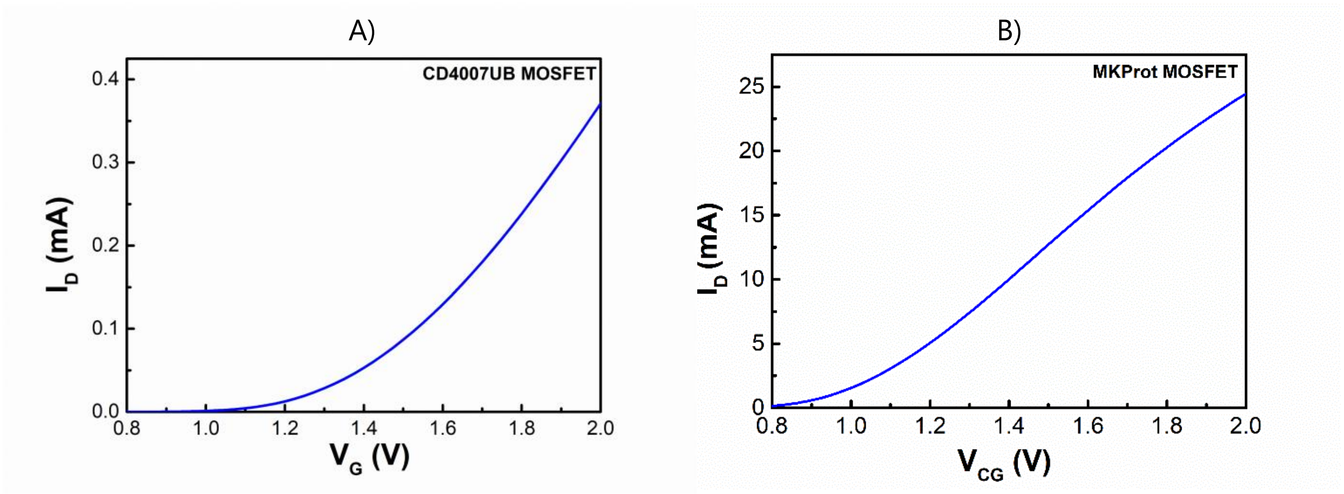

Figure 4.4: Transfer characteristics curves: A) for CD4007UB MOSFET; B) for MKProt MOSFET.

As observed in the images of Figure 4.4, the commercial MOSFET CD4007UB exhibits a transfer curve ranging from a minimum drain current of 51.6 nA to a maximum of 370.7 µA (figure 4.4.A)). In contrast, the transfer characteristic of the custom MKProt MOSFET revealed a significantly broader operational range, with the drain current spanning from a minimum of 145.1 µA to a maximum of 24.5 mA (figure 4.4.B)). These measurements exhibit no variation during 5 consecutive tests, indicating the stable operation of the MOSFETs when analyzed independently. This stability is crucial for ensuring consistent and reliable sensor performance. In this way, the use of the MKPROT MOSFET will result in an increase in the drain current by approximately 66 times. This broader range highlights the enhanced performance of the MKProt, making it better suited for the project's requirements by providing greater sensitivity and operational flexibility.

4.2.2 Analysis of Sensor's Response to pH Solutions

The measurement protocol was executed to test both MOSFETs integrated into the circuit under similar conditions, aiming to identify the optimal sensor testing methodology for sensitivity extraction. The results obtained from extracting sensitivity via transfer characteristics were compared to those derived from real-time analysis. This comparison allowed for a deeper understanding of each method's effectiveness in capturing the sensor's response to pH changes, providing insights into which approach is more reliable and accurate for determining the sensitivity of the CMISFET sensors. Error bars are included to represent the variability in the data across different measurements.

For the signal extraction of the transfer curves, a sequence of pH values (pH 10 → pH 7 → pH 4) was followed in order to increase the protons in the sensor surface. For real-time continuous monitoring of the drain current, a complete cycle was performed with the sequence pH 10 → pH 7 → pH 4 → pH 7 → pH 10. This protocol allowed for a detailed comparison of the performance of both the commercial CD4007UB and the custom MKProt MOSFETs in terms of their response to varying pH levels, ensuring a thorough assessment of their capabilities in the application.

4.2.2.1 Commercial MOSFET CD4007UB (Agilent SPA)

Initially, the sensor integrated with the commercial MOSFET CD4007U was tested. From the following Figure 4.5, it is possible to observe the test setup, where the sensor is placed inside the connector ensuring good electrical contact. This connector is connected to the MOSFET via a breadboard and the MOSFET terminals are connected to the SMU ports of the system test fixture 16442A.

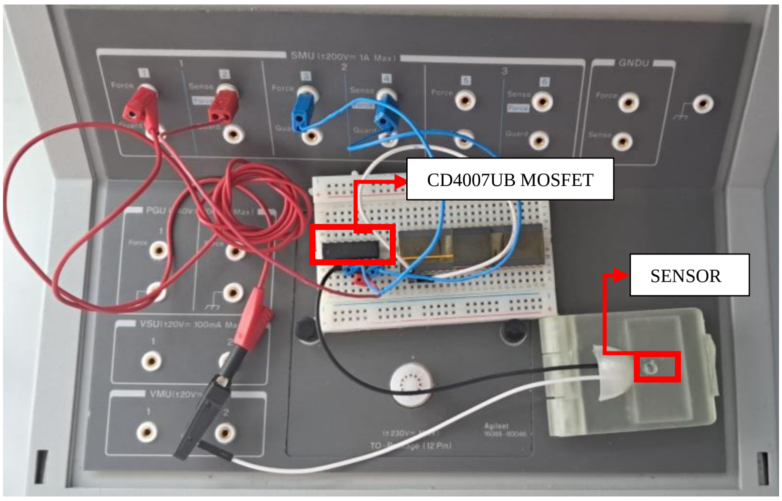

Figure 4.5: CMISFET measurements setup with MOSFET CD4007UB connected.

Firstly, it is presented both analysis, transfer curves and real-time monitoring of the drain current, for the commercial MOSFET CD4007UB in the following images in Figure 4.6.

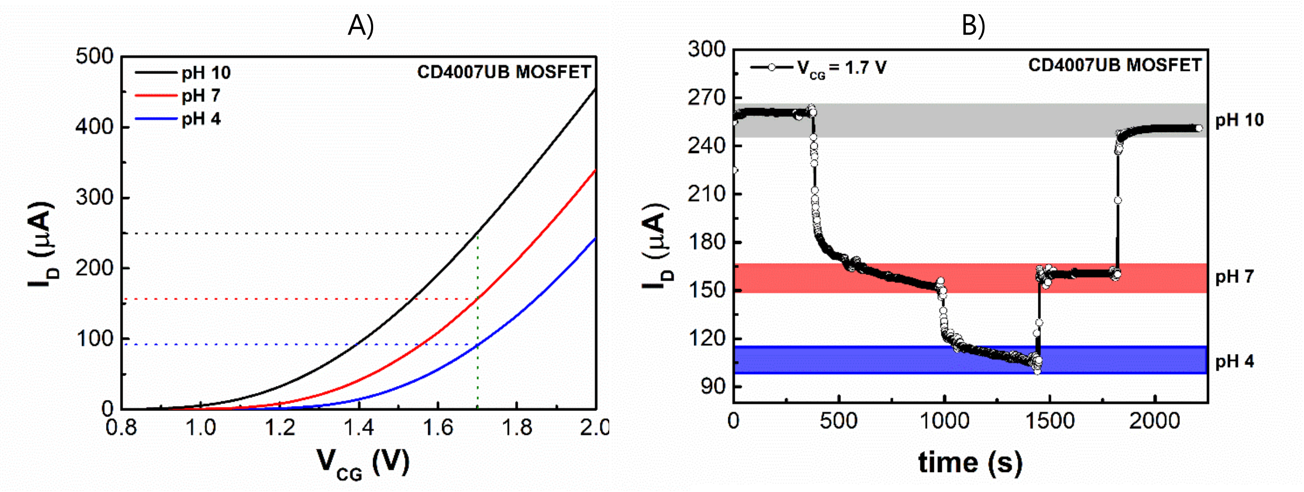

Figure 4.6: pH sensing performance of a tested sensor for CD4007UB MOSFET, evaluated through: A) transfer characteristics with V_D = 0.5 V; B) continuous real-time response of the drain current I_D at a fixed control gate voltage of V_{CG} = 1.7 V.

As noted in both graphs in Figure 4.6, the drain current (I_D) increases with higher pH values. This change in current with varying pH solutions occurs due to charge induction at the surface of the sensitive layer. In this specific topology, charge induction happens directly at the bottom electrode. Consequently, as the proton concentration increases (corresponding to a lower pH), there is a variation in the surface potential of the Ta_2O_5 sensitive layer. This shift in surface potential leads to a decrease in the drain current (I_D), highlighting the sensor's response to different pH levels. This effect demonstrates the sensor's ability to detect pH variations by translating changes in proton concentration into measurable electrical responses.

It can be observed from the real-time monitoring, as shown in Figure 4.6.B), that the sensor's response demonstrates good recovery in terms of drain current, with variations smaller than 20 µA. The transition time was longer, in this case, when the proton concentration increased (lower pH), though this behaviour was not consistent across all sensors. This variation, associated with the hysteresis of the sensor, could be attributed to differences in the pH solution and the volume of the newly introduced solution. To minimize the transition time and mitigate the effects of hysteresis, the cleaning procedure was repeated 3 to 5 times. The cleaning procedure consists in the extraction of the solution in the sensor surface and then, pipetting the new pH solution. This repetition ensured a more consistent sensor response and helped reduce delays in reaching equilibrium, ultimately improving the accuracy and reliability of the sensor's real-time monitoring performance. In general, hysteresis is observed during transitions to pH 4, which is influenced by the point of zero charge (pHpzc) of the sensitive oxide layer. The point of zero charge (pHpzc) represents the pH at which the surface of the oxide layer carries no net electrical charge, meaning the number of positively and negatively charged surface groups is equal. When the pH shifts away from this point, charge accumulation on the surface occurs, potentially inducing hysteresis effects. This phenomenon is particularly prominent in lower pH environments, such as pH 4, where it can impact the sensor's response and stability during pH transitions. In the case of tantalum pentoxide (Ta_2O_5), the pHpzc typically falls within the range of 4 to 5. [35],[36]

To extract the sensitivities from both methods of analysis (transfer curves and real-time monitoring), the drain current was plotted against the pH value at a fixed control gate voltage (V_{CG}) of 1.7V for both cases in Figure 4.8. This approach allowed for a direct comparison of the sensor's response to varying pH levels, enabling the evaluation of sensitivity across different pH ranges for both methods.

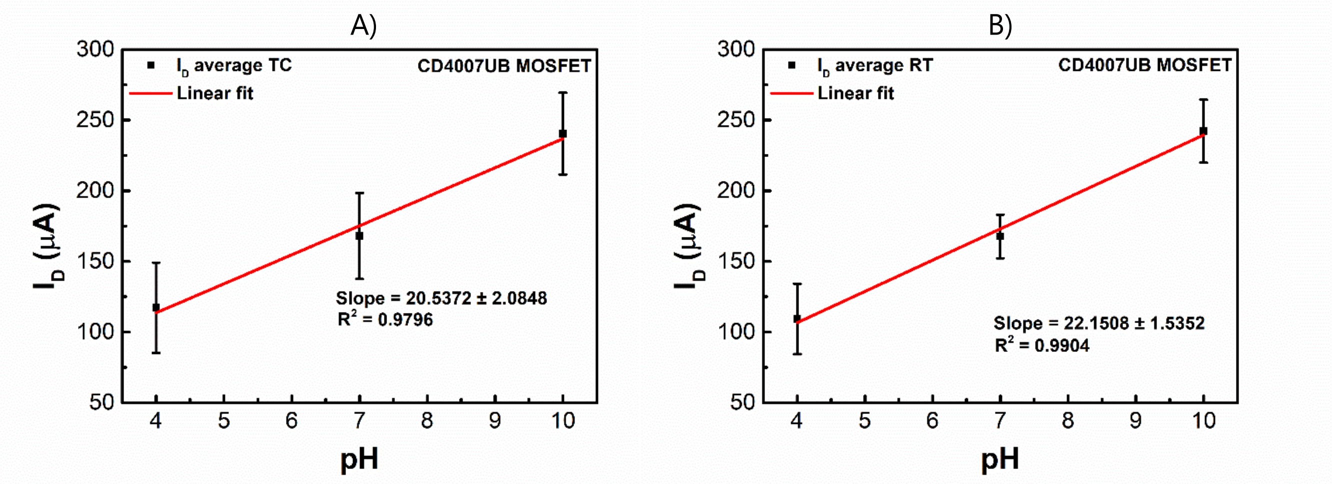

Figure 4.8: Sensitivity extracted for CD4007UB MOSFET for pH testing: A) from transfer curves; B) from real-time monitoring.

When comparing the results of both analysis methods from the previous graphs in Figure 4.8, it is evident that the sensitivity obtained from real-time monitoring (Figure 4.8.B)), determined by the slope of the linear fit (sensitivity = 22 ± 1 µA/pH), is similar to the sensitivity extracted from the analysis of the transfer curves (sensitivity = 21 ± 2 µA/pH) (Figure 4.8.B)). It is also possible to observe from the figure that the measurements exhibit significant variability, as indicated by the error bars, particularly in the case of the measurements conducted during the transfer curves. This variability arises because the analysis was performed considering all the tested sensors, which demonstrate a high degree of variability among themselves. This variability can be further illustrated in the following Figure 4.7 which compiles the curves recorded for all the tested sensors.

The variation between sensors' behaviour may be attributed to inconsistencies in the deposition of the various layers, leading to variations in sensor performance. This variability poses a challenge to the overall reliability of the sensors, especially when aiming for consistent and accurate measurements. Despite the testing setup and methodologies applied, the sensors' sensitivity exhibited a wide range of responses, making it difficult to achieve uniform and reproducible results across all samples. Further optimization of the fabrication process and careful calibration of each sensor might be necessary to reduce this variability and enhance the performance consistency of the system.

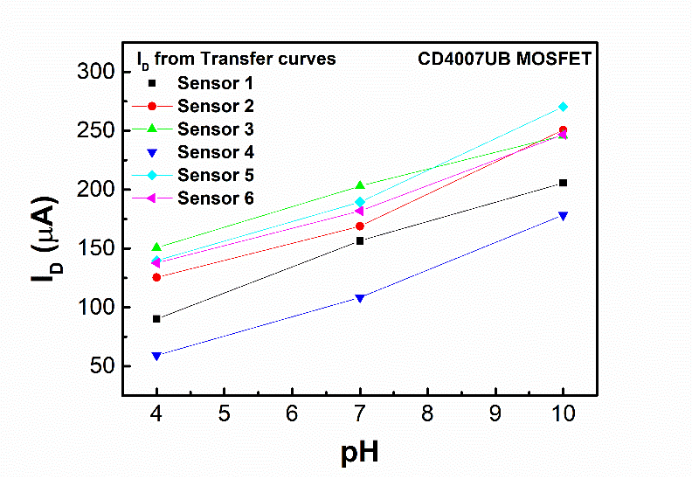

Figure 4.7: Variability of sensor measurements for transfer curves analysis for 6 different sensors.

Another comparative method for evaluating sensitivity is the graphical representation of the normalized drain current I_D with sample pH, denoted as ΔI_D (pH10-pHx). This method allows for a direct comparison of the current response at different pH levels by normalizing the change in I_D concerning a reference pH, in this case, pH 10. By analyzing the normalized current variations, we can better understand the relative performance of different sensors or connection topologies under varying pH conditions, enhancing the interpretation of sensitivity trends across a range of pH values. However, the main downside of this comparative analysis method is the loss of information regarding the error associated with pH 10 measurements, as pH 10 is used as the reference point. Nonetheless, the pH 10 solution is always the first to contact the sensing electrode in each new cycle and is given more time to stabilize, thereby minimizing hysteresis effects between cycles and promoting more consistent measurements within the same sensor. This consistency makes the pH 10 buffer a reliable reference for comparative analysis, despite showing more significant errors between different sensors, even with the slight trade-off in error representation.

This comparative method was performed for both methods of analysis as can be seen in the following Figure 4.9.

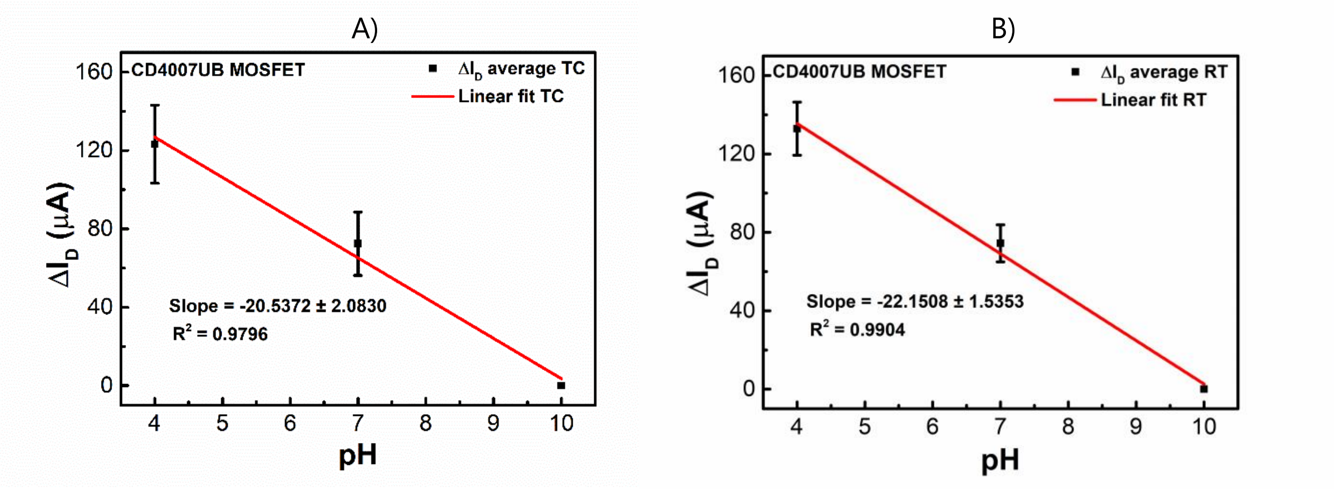

Figure 4.9: Sensitivity extracted for CD4007UB MOSFET from average ΔID for pH testing: A) from transfer curves; B) from real-time monitoring.

As can be observed from the graph in Figure 4.9, the sensitivities extracted using this method are similar to those previously obtained directly from both the transfer curves (Figure 4.8.A)) and real-time measurements (Figure 4.8.B)) with a fixed V_{CG}. The sensitivities are 21 ± 2 µA/pH and 22 ± 2 µA/pH, respectively, demonstrating consistency across the different analysis methodologies. The errors in the real-time monitoring are less significant, indicating that real-time monitoring offers improved accuracy and consistency for pH sensing making it a more reliable approach for sensor performance evaluation. The greater variation observed in the transfer characteristics extraction method may stem from several factors. One possibility is that each time a transfer curve is acquired, stress is induced in the MOSFET, potentially leading to inherent variation over time. Additionally, real-time monitoring provides a clearer understanding of drift tendencies and stabilization periods, thereby enhancing measurement reliability. This method allows for the observation of transition trends, enabling the acceleration of speed and stabilization by cleaning the sensor with the desired solution as needed. This proactive approach helps maintain optimal sensor performance and minimizes measurement inconsistencies.

Comparing with the previous method described in Figure 4.8, there was no significant improvement in terms of measurement variability. The sensors exhibited a considerable degree of variation in their performance, both in terms of the maximum current recorded and their sensitivity.

Since in the literature, the sensitivities of sensors are usually represented in voltage per pH values, an analysis was performed using the characteristic transfer curves by fixing the current value at approximately 50% of the maximum current recorded for each sensor analysis. The following Figure 4.10 illustrates the sensitivity extracted using this metric, as expressing sensitivity in mV/pH is the most common approach to evaluate device performance in existing studies. This method allows for a standardized comparison with other sensors reported in the literature and with the custom-made MOSFET MKProt, facilitating a clearer assessment of the sensor's efficacy in practical applications.

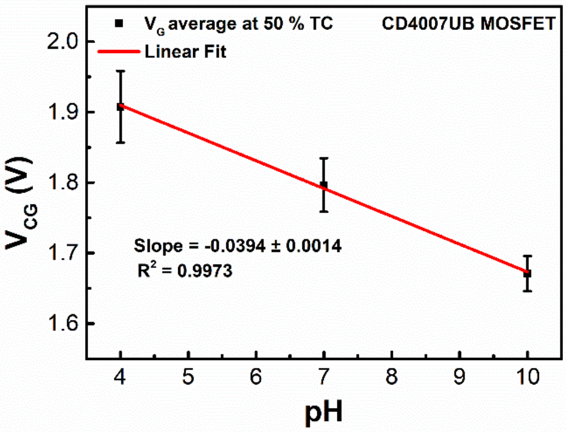

Figure 4.10: Sensitivity extracted for CD4007UB MOSFET at a fixed value of the transfer curve (50%) for pH testing.

Similarly to the previous sensitivity extractions, it can be observed from the slope of the linear fit of Figure 4.10 that the sensitivity for the sensor in the circuit with the commercial MOSFET CD4007UB is equal to 39 ± 1 mV/pH.

4.2.2.2 Developed MOSFET MKProt (Agilent SPA)

From the following Figure 4.11, it's possible to observe the test setup with the MOSFET MKProt integrated, in a similar way as the previous one. This connector is connected to the MOSFET via a breadboard and the MOSFET terminals are connected to the SMU ports of the system test fixture 16442A.

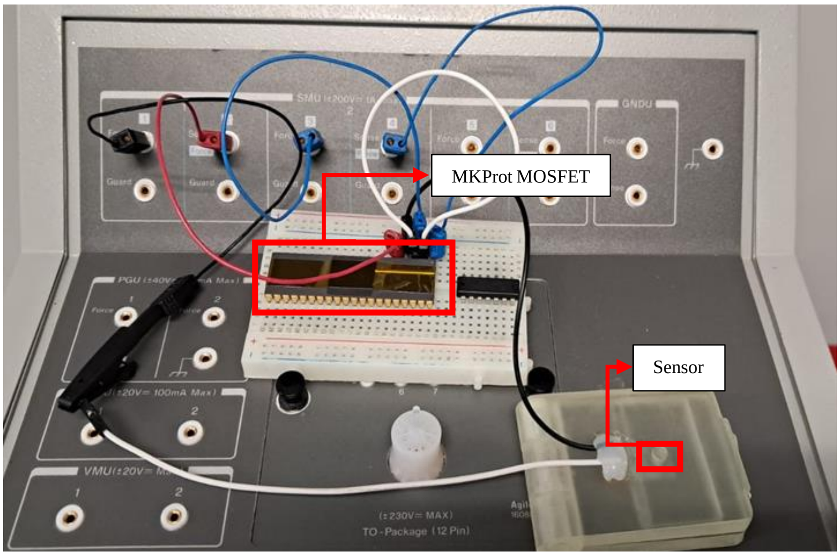

Figure 4.11: CMISFET measurements setup with MOSFET MKProt connected.

As previously mentioned, the pH solution analyses were conducted for both MOSFETs integrated into the circuit, CD4007UB and MKProt, to compare which would demonstrate better performance in terms of sensitivity. The following section will present the analyses conducted with the MKProt MOSFET, allowing for a more detailed evaluation of its behaviour and performance in comparison to the commercial MOSFET.

This evaluation aimed to determine whether the custom MKProt offered improvements in sensor performance, sensitivity, and reliability, and to identify any advantages it held over the commercially available MOSFET in terms of aligning with the specific requirements of the monitoring system. Through this, it becomes possible to assess if the custom MOSFET design is better suited for real-time, on-site measurements, while providing higher accuracy and consistency, especially in challenging environments.

Firstly, the transfer curves and real-time continuous monitoring of the drain current are presented in the following images in Figure 4.12.

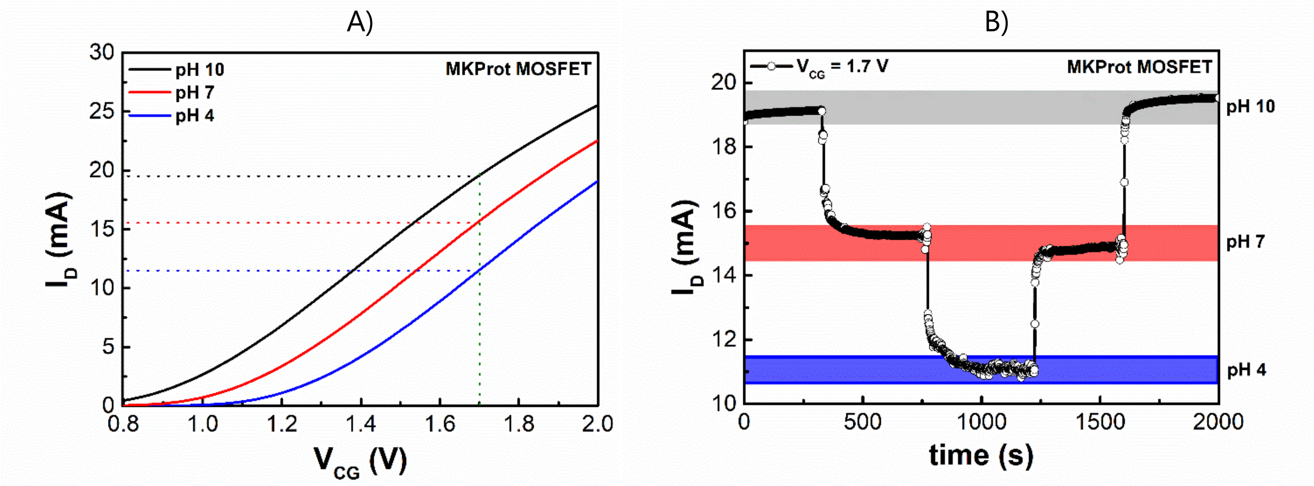

Figure 4.12: pH sensing performance of a tested sensor for MKProt MOSFET, evaluated through: A) transfer characteristics with V_D = 0.5 V; B) continuous real-time response of the drain current I_D at a fixed control gate voltage of V_{CG} = 1.7 V.

As noted in previous Figure 4.12, analogous to the MOSFET CD4007UB (Figure 4.6), the drain current (I_D) increases with higher pH values in the MKProt MOSFET as well, as this change in current occurs due to charge induction at the surface of the sensor's sensitive layer. The interaction between the pH solution and the sensitive layer induces charges at the sensor surface, which directly affects the channel current.

It can be observed from the real-time monitoring (as shown in Figure 4.12.B) that the sensor's response also demonstrates a good recovery in terms of drain current, with variations in the order of less than 1 mA. The duration of the real-time cycle for this analysis was shorter than that observed for the CD4007UB MOSFET analysis. However, this difference is not very significant and cannot be solely attributed to the MOSFET's performance, as the sensing layer of the sensors fabricated on the PEN substrate shows considerable variability in this regard, as noted in Figure 4.7. This variability can influence the overall response time and recovery of the sensors, making it essential to consider other factors beyond just the MOSFET type when evaluating performance. However, the fact that the sensor's response translates into higher voltage values enhances the readability of the analysis performed. This is particularly advantageous concerning the project's primary objective: designing a portable and reliable device for on-site measurements. Clear and interpretable voltage readings facilitate user engagement and improve the overall effectiveness of the device in real-world applications.

To extract the sensitivities from both methods of analysis (transfer curves and real-time monitoring) for the MKProt MOSFET, the same approach used for the CD4007UB MOSFET was applied, focusing on the current deltas relative to the reference value corresponding to the pH 10 buffer solution. The deltas of drain current were plotted against the pH value at a fixed control gate voltage (V_{CG}) of 1.7V for both cases in Figure 4.13. A). Similarly to the analysis performed earlier, it was also plotted the sensitivity in terms of voltage as a function of pH in Figure 4.13. B) to obtain a more direct comparison with the literature and among the MOSFETs.

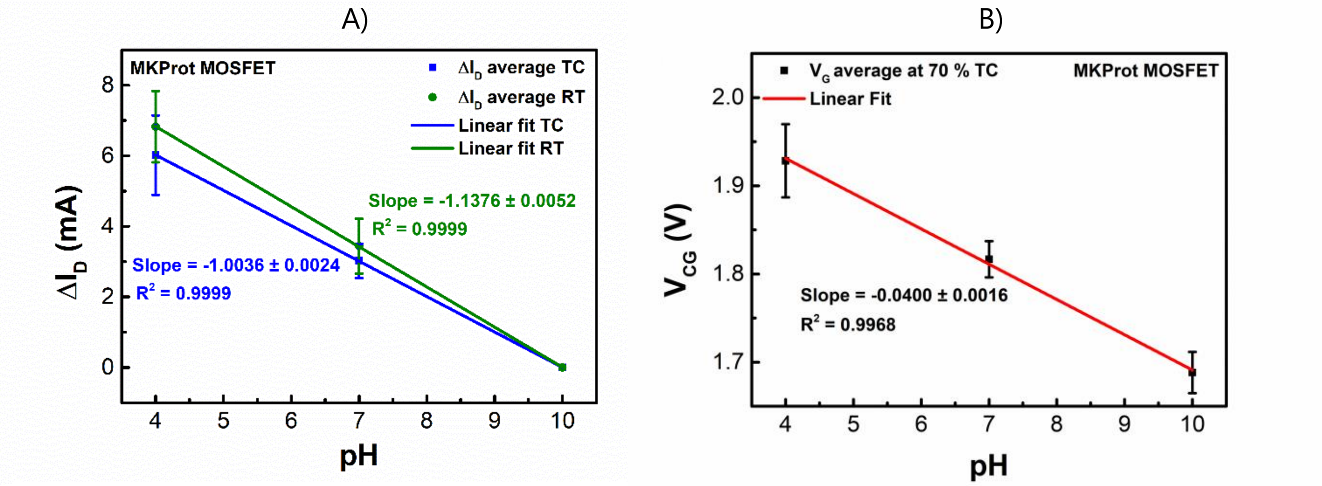

Figure 4.13:A) Sensitivity extracted for MKProt MOSFET from average ΔID for pH testing: blue) from transfer curves; green) from real-time monitoring. B) Sensitivity extracted for MKProt MOSFET at a fixed value of the transfer curve (70%) for pH testing.

When comparing the results of both analysis methods, the sensitivity obtained from real-time monitoring (green), determined by the slope of the linear fit of the graph of Figure 4.13.A) (sensitivity = 1.14 ± 0.01 mA/pH), is higher than the sensitivity extracted from the transfer curve analysis (blue) (sensitivity = 1.02 ± 0.01 mA/pH).

Unlike the previous analysis for MOSFET CD4007UB, in Figure 4.13.B), the drain current values were fixed at approximately 70% of the maximum value of the transfer curve for all sensors. This difference in fixing the value is due to the distinct shapes of the curves, as the sensor with the MKPROT MOSFET does not exhibit as steep a rise in current as that of the CD4007UB. By selecting a point that better reflects the operational characteristics of the MKProt, it is possible to ensure that comparisons between the two MOSFETs are more relevant to their respective performances in real-world applications. From the linear fitting of the graph in Figure 4.13.B), it is possible to extract the sensitivity value in terms of voltage per pH. Thus, it is possible to record a value of 40 ± 2 mV/pH.

4.2.2.3 Microfluidic Setup (Agilent SPA)

Previous studies revealed that the solution deposition frequency influences the sensor's measurements, and therefore a microfluidic system was designed to improve control over the deposition process and provide more consistent fluid delivery to the sensor surface. This system was integrated into the testing setup with the MOSFET MKProt (Figure 4.14) to compare its performance with the results obtained from manual solution deposition, allowing for a more detailed evaluation of how the frequency and consistency of solution application affect the sensitivity and accuracy of the pH measurements.

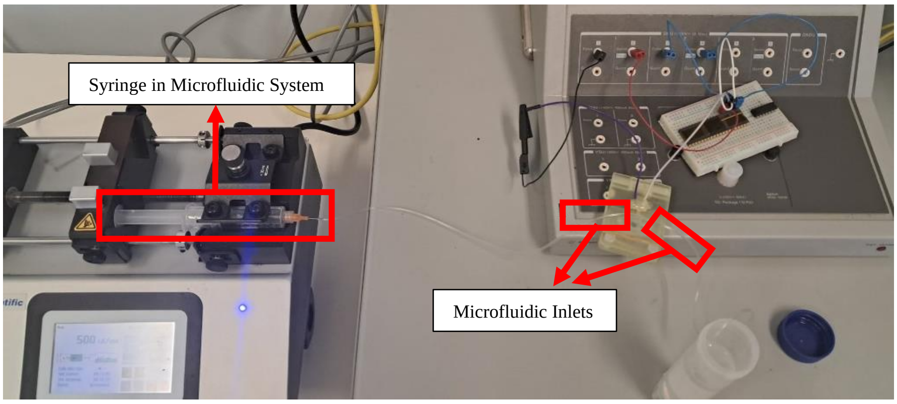

Figure 4.14: CMISFET measurements setup with Microfluidic system with MOSFET MKProt connected.

This microfluidic system also provides the advantage of preventing sensor wear and tear that might occur due to minor physical contact with the sensitive area during manual solution changes. By automating the solution deposition, the system ensures more consistent application and reduces the risk of damage, contributing to improved sensor longevity and maintaining the integrity of the measurements over time.

In this way, the measurements and extraction of sensitivities were performed in a manner consistent with the previous methods, these being presented in the following Figure 4.15.

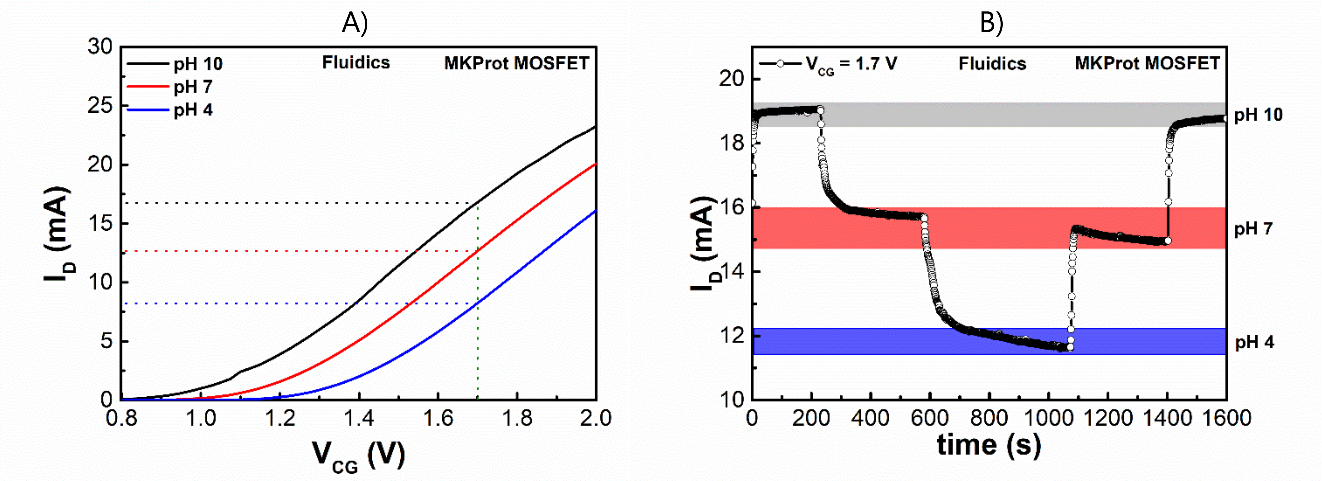

Figure 4.15: pH sensing performance of a tested sensor for MKProt MOSFET for microfluidic system, evaluated through: A) transfer characteristics with V_D = 0.5 V; B) continuous real-time response of the drain current I_D at a fixed control gate voltage of V_{CG} = 1.7 V.

As observed in previous analyses, Figure 4.15 the behaviour indicates a decrease in proton concentration at the sensitive layer, which directly affects the surface potential. The reduced proton presence in higher pH solutions leads to less induction at the sensor's bottom electrode, thereby increasing the channel current in response to the changing chemical environment. It can be observed from the real-time monitoring, Figure 4.15.B), that the sensor's response demonstrates a good recovery in terms of drain current. However, the transition between pH 4 and pH 7 reveals the influence of hysteresis. During this transition, the time required for stabilization was longer, and the current recovery was weaker compared to other pH transitions. This suggests that the sensor experiences more pronounced lag or memory effects when transitioning between these particular pH levels. This behaviour can be attributed to the point of zero charge (pHpzc) of the tantalum oxide (Ta_2O_5) sensitive layer.

Next, the plot of the comparative method between the transfer curves and real-time data, focusing on the current deltas relative to the reference value corresponding to the pH 10 buffer solution was performed.

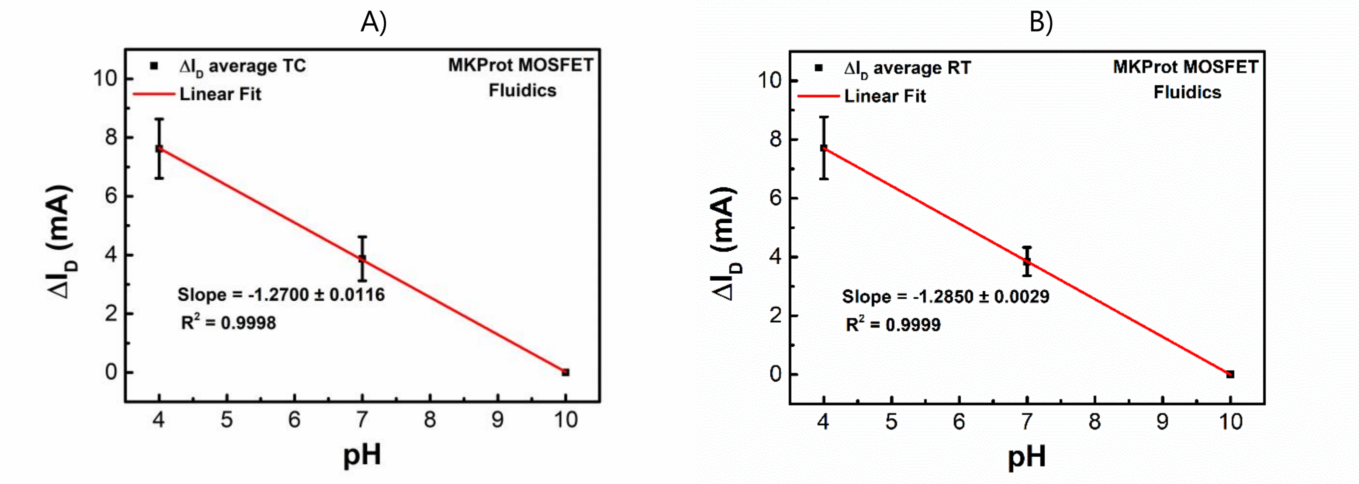

Figure 4.16: Sensitivity extracted for MKProt MOSFET fluidics system from average ΔI_D for pH testing: A) from transfer curves; B) from real-time monitoring.

Through the graphs in Figure 4.16, it’s possible to extract the sensitivities using this method from the average deltas currents to a reference value of the current of pH 10. The extracted sensitivities are 1.27 ± 0.01 mA/pH and 1.285 ± 0.003 mA/pH, for transfer curve analysis and real-time monitoring, respectively.

This extracted sensitivities for the microfluidics system show a significant increase compared to the manual deposition testing setup with the MKProt MOSFET. This improvement highlights the effectiveness of the microfluidic approach in enhancing sensor performance and reliability, providing more consistent and higher sensitivity measurements.

For the plot of voltage as a function of pH value, the drain current values were fixed at around 70% of the maximum current observed in the transfer curves. This comparison will help evaluate the performance of the microfluidic system in relation to the traditional methods used in earlier experiments.

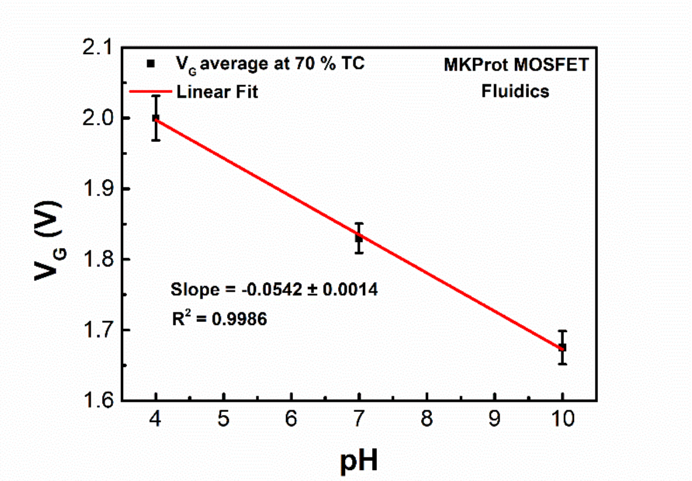

Figure 4.17: Sensitivity extracted for MKProt MOSFET for microfluidics system at a fixed value of the transfer curve (70%) for pH testing.

From the linear fitting of the graph of Figure 4.17, the sensitivity value in terms of voltage per pH can be extracted. The recorded value is 54 ± 1 mV/pH, which is significantly higher than the previous sensitivities extracted for both MOSFETs during manual deposition of the buffer solutions and close to the theoretical limit of 59.2 mV/pH. This enhanced sensitivity for the microfluidics system underscores the effectiveness of the microfluidic approach in improving sensor performance, resulting in more sensitive measurements. The increased sensitivity may be attributed to the controlled and efficient delivery of solutions, which minimizes disturbances and enhances the sensor's response to pH changes. This constant deposition of new solution prevents any part of the solution from drying, ensuring a consistent and stable environment for the sensor. This stability allows for more accurate measurements and quicker responses to variations in pH, ultimately leading to improved sensor performance in detecting changes.

In Table 4.1 below, sensitivity values from all methodologies are compiled to enable a comparison between the two different MOSFETs. This comparison also highlights the differences in sensor performance when using manual solution deposition versus the custom-designed microfluidic system for the project.

Table 4.1: Summary of the sensitivities results obtained for both MOSFETs (CD4007UB and MKProt) and microfluidics system.

	Sensitivity TC ΔI_D	**Sensitivity RT ΔI_D**	**Sensitivity TC I_{REF} (mV/pH)**
MOSFET CD4007UB	21 ± 2 µA/pH	23 ± 2 µA/pH	39 ± 1
MOSFET MKProt	1.004 ± 0.002 mA/pH	1.14 ± 0.01 mA/pH	40 ± 2
Microfluidics system (MKProt)	1.27 ± 0.01 mA/pH	1.285 ± 0.003 mA/pH	54 ± 1

By examining these results from Table 4.1, it’s possible to determine if the new approaches offer improvements in sensitivity and overall detection capabilities.

For most of the sensitivity values extracted for both MOSFETs, a direct comparison is not feasible once the MKProt MOSFET amplifies the signal, leading to significantly higher sensitivity values, however, its noted a better precision of results for this developed MOSFET. When using the manual solution deposition methodology, a comparison in terms of the metric mV/pH shows that the sensitivities are similar between the different MOSFETs.

When the microfluidic system methodology is employed, there is a noticeable increase in sensitivity across all measured values. This suggests that the microfluidic method not only enhances sensitivity but also provides other benefits, such as preventing direct contact with the sensor, which could improve sensor stability and longevity. The sensitivity achieved using the microfluidic system, 54 ± 1 mV/pH, approaches the theoretical limit for an ideal sensor as described by Nernst's law, which is 59.2 mV/pH at 298 K. This proximity to the theoretical limit indicates that the microfluidic system significantly improves the sensor's performance, demonstrating an increase of approximately 35% when compared to manual deposition method.

4.2.2.4 CMISFET controller board

To design a user-friendly and accessible device that eliminates the need for laboratory testing while maintaining the reliability of the results, a controller board and software were developed in a previous master's thesis. The software allows for direct data collection and visualization on-site while connected to a controller PCB that is attached to an Arduino board and the sensor, as shown in Figure 4.18.

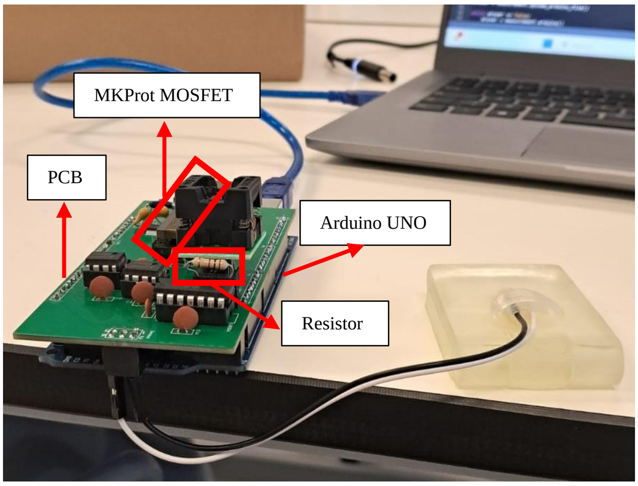

Figure 4.18: Testing Setup with CMISFET controller Board.

The analyses performed using the developed Controller Board were conducted with pH solutions to assess the reliability of the device and to compare the results with those obtained using the Agilent 4155C semiconductor parameter analyzer during electrical characterization. To carry out the voltage sweeps, several key parameters need to be defined: Initial and final V_{CG} voltages (0.2-1.4 V); V_D voltage (0.5 V); Number of voltage steps (5); and Number of points per step (1). For continuous real-time monitoring, a fixed V_D value (0.5 V) must be defined and the VCG voltage needs to be set, which is determined based on the previous voltage sweep analysis.

The pH solution analysis was conducted by altering a key resistor in the PCB circuit (Appendix A.4), which effectively modelled the sensor's behaviour and enabled readings via the Arduino microcontroller. Three different resistors (30kΩ, 1kΩ and 460Ω) were tested to determine which would provide the most accurate and reliable performance for this specific type of analysis. Each resistor affected the voltage drop across the circuit and, thus, the output read by the Arduino. By experimenting with various resistor values, it was possible to fine-tune the circuit to better reflect the sensor’s real-time response to changes in pH, ensuring that the selected resistor offered the best match for the electrical characteristics of the CMISFET sensor. This iterative testing allowed for optimization of the PCB setup, improving the accuracy and reliability of on-site measurements compared to the controlled lab environment.

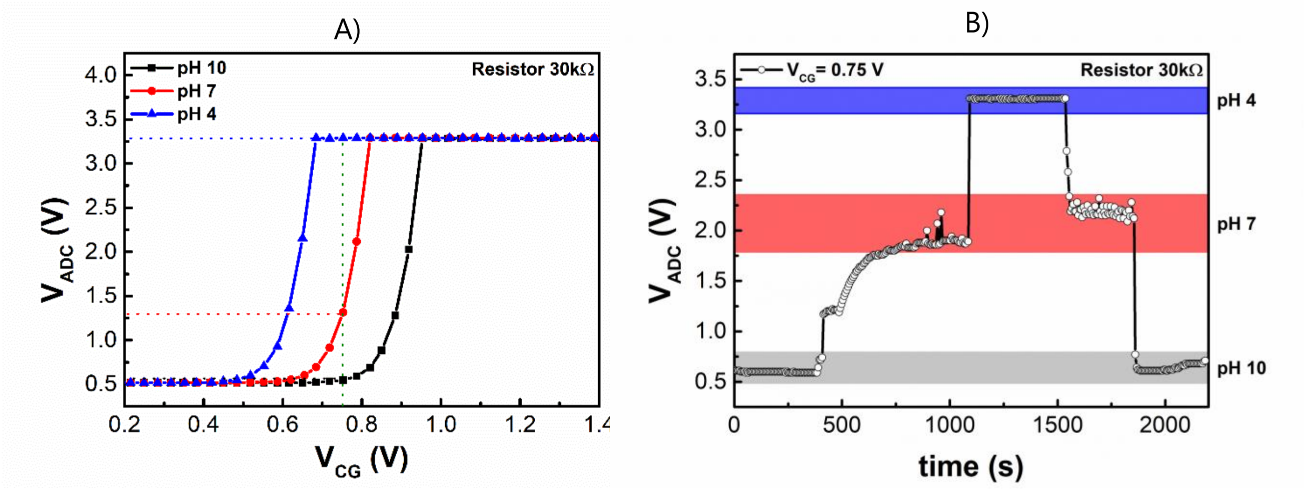

Figure 4.19: pH sensing performance of a tested sensor for developed Controller Board for 30kΩ resistor, evaluated through: A) voltage sweeps with V_D = 0.5 V; B) continuous real-time response of the drain current I_D at a fixed control gate voltage of V_{CG} = 0.75 V.

As can be observed from the graphs in Figure 4.19, the behaviour of this methodology is contrary to what was previously observed in the analyses conducted with the Agilent 4155C. This is because the PCB was designed with the understanding that the sensor exhibited better sensitivity when charge induction occurred at the bottom electrode. Thus, the signal is converted to show an increase in current with a decrease in pH value, meaning an increase in proton concentration on the sensor's surface.

Since the current increase from the threshold voltage (V_T) is quite steep for this resistor value (30kΩ), it becomes challenging to identify a control gate voltage (V_{CG}) at which real-time analysis can be conducted without reaching saturation at the maximum analog-to-digital converter (V_{ADC}) value read by the Arduino. As shown in the figure, there is a forced stabilization of the sensor's behaviour for the pH 4 solution, indicating that the device is unable to read values exceeding 3.3V. This saturation limits the effective range of the sensor and necessitates adjustments in the experimental setup to ensure accurate measurements without hitting the maximum voltage. Given this fact, any sensitivity calculations, for this resistor, based on these measurements may lead to misleading conclusions about the sensor's performance. Adjustments to the circuit or the experimental parameters will be necessary to obtain reliable sensitivity values.

Thus, two additional resistors were tested to determine which would be suitable for this experiment, and the data for the 1kΩ resistor is presented below in Figure 4.20.

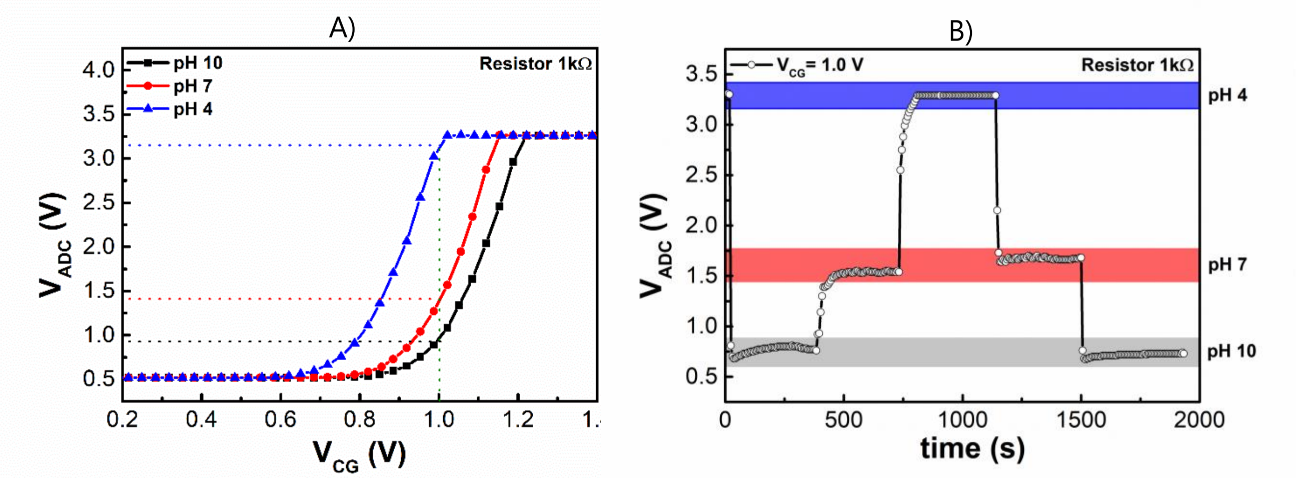

Figure 4.20: pH sensing performance of a tested sensor for developed Controller Board for 1kΩ resistor, evaluated through: A) voltage sweeps with V_D = 0.5 V; B) continuous real-time response of the drain current I_D at a fixed control gate voltage of V_{CG} = 1.0 V.

It can be observed from Figure 4.20 that the behaviour for this 1kΩ resistor is similar to the previous one, again presenting some difficulty in establishing a V_{CG} value that maximizes sensitivity while remaining within the voltage limits readable by the Arduino microcontroller. The steep current increase near the Vt value indicates that small changes in the gate voltage led to significant variations in the current response, especially in the transition to pH4, which results in saturation.

To address this challenge, the analogous analysis was also conducted for the 460Ω resistor.

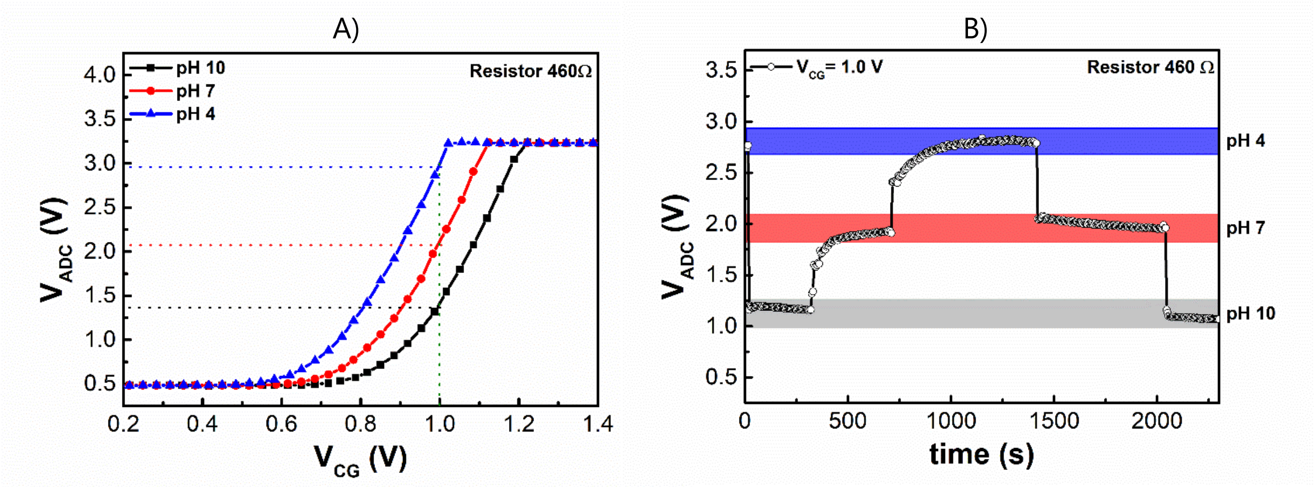

Figure 4.21: pH sensing performance of a tested sensor for developed Controller Board for 460Ω resistor, evaluated through: A) voltage sweeps with V_D = 0.5 V; B) continuous real-time response of the drain current I_D at a fixed control gate voltage of V_{CG} = 1.0 V.

In this case, it can finally be observed from Figure 4.21 that it is easier to define a V_{CG} voltage for real-time measurement, with a value established at 1.0V, as this maximizes the sensor's sensitivity concerning the buffer pH solutions. The successful establishment of a V_{CG} voltage at 1.0V in Figure 4.21.B), represents a significant step in optimizing the sensor's performance for real-time pH monitoring. The sensitivity results will be crucial for evaluating the effectiveness of the device in practical applications. Further tests and validations should be conducted to reinforce the findings and ensure reliability in various environmental conditions.

Thus, the determination of sensitivities extracted from transfer curves and real-time analysis for the device with a resistor value of 460Ω is presented below in Figure 4.22. The extracted sensitivities are performed for the deltas of V_{ADC}, as it was verified earlier that this method is the most effective for extracting sensitivity values, once this approach accurately represents the behaviour of the sensor in a more consistent manner.

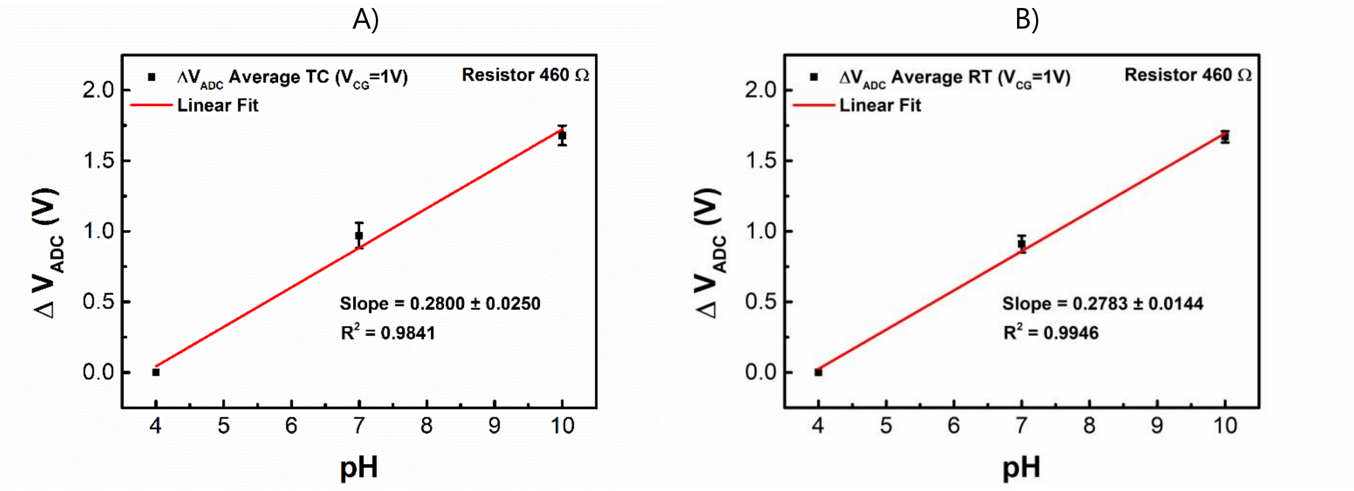

Figure 4.22: Sensitivity extracted from average ΔV_{ADC} for pH testing in developed Controller Board for 460Ω resistor: A) voltage sweeps; B) from real-time monitoring.

It is possible to extract, from the graphs in Figure 4.22, the sensitivities based on the ΔV_{ADC} determined from the transfer curves, Figure 4.22.A), and real-time analysis, Figure 4.22.B) recording values of 0.28 ± 0.03 V/pH and 0.28 ± 0.01 V/pH, respectively. These sensitivity values are quite similar to each other; however, the value extracted from the real-time analysis showed less measurement error, indicating a more consistent and reliable performance for real-time monitoring compared to the transfer curve analysis.

Next, to compare with the sensitivities extracted from the Agilent 4155C, a plot of voltage as a function of pH was created to enable a more direct comparison between methodologies and the literature. The drain current values were fixed at approximately 70% of the maximum value observed in the transfer curves for all sensors, to maximize this sensitivity value. This method provides clarity in assessing the sensor's performance across different testing environments and setups.

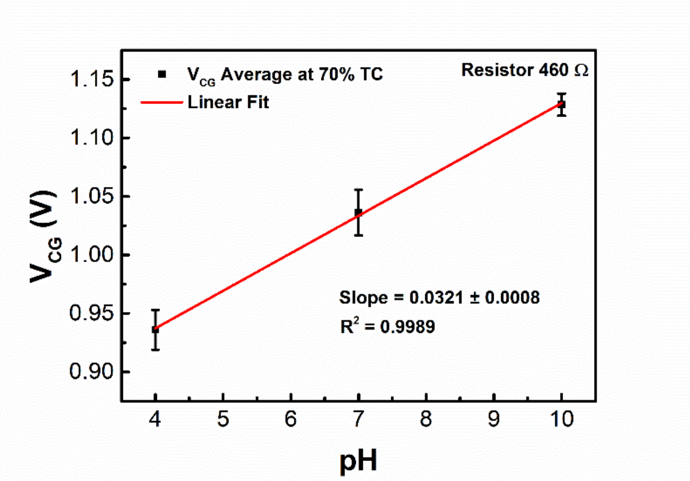

Figure 4.23: Sensitivity extracted for developed Controller Board at a fixed value of the voltage sweep (70%) pH testing.

From the linear fitting of the graph of Figure 4.23, the sensitivity value in terms of voltage per pH can be extracted. The recorded value is 32.1 ± 0.8 mV/pH.

The values for tests conducted on pH solutions are recorded in the following table. This analysis will assess whether the developed Controller Board is suitable for pH analysis and, consequently, for detecting heavy metals in solution.

Table 4.2: Summary of the sensitivities and comparison of results obtained for pH testing with MKProt MOSFET, in the developed Controller Board and Agilent 4155C SPA.

	Sensitivity VS/TC ΔV_{ADC} /ΔI_D	**Sensitivity RT ΔV_{ADC} /ΔI_D**	**Sensitivity VS/TC 70% (mV/pH)**
CMISFET Controller Board	0.28 ± 0.03 V/pH	0.28 ± 0.01 V/pH	32.1 ± 0.8
Agilent 4155C (MKProt)	1.004 ± 0.002 mA/pH	1.14 ± 0.01 mA/pH	40 ± 2

As observed in the previous Table 4.2, the sensitivity results from measurements taken with the custom PCB and software cannot be directly compared to those obtained with the Agilent 4155C, as these measurements are expressed in different units. The custom software records all measurements in terms of voltage, while the Agilent analyzes current. Therefore, the only directly comparable values are those obtained from the voltage sweeps or transfer curves, where V_{CG} values are extracted for both systems.

Although the sensitivity value obtained from the custom system is lower (32.1 ± 0.8 mV/pH) than for Agilent 4155C testing, it is still within the expected range, demonstrating the effectiveness of the measurements taken with this setup. This finding indicates that the custom system is reliable for future analyses, particularly in the context of heavy metal detection.

4.2.3 Detection of heavy metals in Agilent SPA

Using the same measurement protocol, the sensors were also tested by exposing the sensitive area to solutions of two different heavy metals: mercury (II) chloride 99% and cadmium chloride hydrate (98%). For these solutions, the transfer curve characteristics and continuous real-time monitoring were conducted with manual deposition in the testing setup using the MKProt MOSFET. The solution exchanges were carried out by gradually increasing the concentration of the deposited solutions. This method aimed to evaluate the sensor's response to varying concentrations of heavy metals and assess its sensitivity and reliability in detecting these contaminants in solution.

Each solution exchange required washing with a new solution approximately five times to stabilize the current value. This stabilization proved to be more challenging to achieve compared to the pH solutions, likely due to the stronger interaction between the heavy metal ions and the sensitive layer of the sensor and since buffer solutions are specifically formulated to maintain a stable pH when small amounts of acids or bases are introduced.

The following sections will present the results and analysis of these tests, highlighting the performance of the MKProt MOSFET in heavy metal detection. The error bars indicate the consistency and repeatability of the sensor's response at various concentrations, highlighting any deviations and providing a clearer understanding of the sensor's sensitivity to different concentrations of heavy metals in solution.

4.2.3.1 Mercury Chloride Solutions

Firstly, the measurements for transfer curves and real-time monitoring were conducted for mercury chloride. The concentrations of this solution used were 1 ppm, 5 ppm, 10 ppm, 15 ppm and 25 ppm. These concentrations were selected because they exhibited a measurable decrease in drain current. The positive charge of mercury ions results in the accumulation of ions on the sensitive surface, leading to these changes in the sensor's response. This allows us to define an approximate limit of detection for the sensor concerning this heavy metal.

The following figures will present the transfer curves and real-time monitoring data, illustrating the correlation between mercury chloride concentrations and the resulting drain current variations.

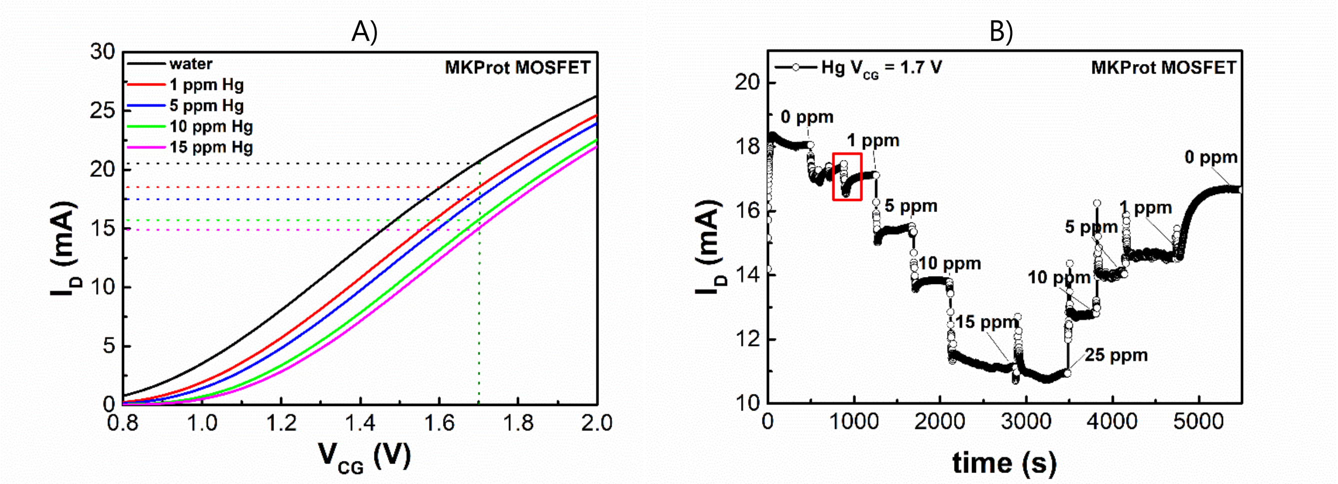

Figure 4.24: Hg solutions sensing performance of a tested sensor for MKProt MOSFET, evaluated through: A) transfer characteristics with V_D = 0.5 V; B) continuous real-time response of the drain current I_D at a fixed control gate voltage of V_{CG} = 1.7 V.

Through the graphs in Figure 4.24, it is possible to observe the decrease in drain current with the increased concentration of the deposited mercury chloride solution. The results indicate a clear trend, where higher concentrations of mercury chloride led to more pronounced decreases in drain current, highlighting the sensor's sensitivity to this heavy metal. The red square in Figure 4.24.B) highlights the moment when an additional 1 ppm solution was introduced to the surface of the sensor. This action was taken in response to the observed significant hysteresis relative to the reference value of distilled water. The introduction of the additional solution aims to mitigate the hysteresis effects and stabilize the sensor's response, allowing for more accurate measurements. From the same Figure 4.24.B), it can be observed that a solution concentration of 25 ppm was also tested, however, this concentration did not exhibit a significant difference in response across all sensors tested especially for transfer curves analysis. This lack of notable change may indicate a saturation point in the sensor's response to mercury chloride, suggesting that concentrations beyond a certain level do not further impact the drain current. The recovery of the signal current when the concentrations are decreased is less effective than in the pH testing. This can be attributed to the saturation of ions on the sensor's surface. As a result, the sensor may take longer to return to baseline levels, highlighting the need for further optimization in the cleaning and stabilization processes when working with heavy metal solutions.

Especially in the analysis of heavy metals, real-time monitoring of the sensor's behaviour provides significant advantages. This approach allows for continuous observation of the sensor's performance, facilitating immediate adjustments to improve stabilization. This dynamic capability enhances the reliability and accuracy of the measurements, making it a valuable tool for assessing the sensor's effectiveness in detecting heavy metal contamination.

Since the sensors did not exhibit satisfactory current recovery, repeated analyses on the same sensor were avoided. Performing multiple tests in the same sensor would likely cause a significant decrease in drain current and lead to sensor degradation due to the accumulation of mercury ions on the sensitive layer, compromising the sensor's functionality. Thus, the following analyses, conducted through transfer curve measurements and real-time monitoring, will demonstrate the average results for three different sensors.

Analogous to the pH analysis, an analysis of the sensor's behaviour in terms of current deltas was performed for the heavy metal testing. By comparing the current deltas relative to the reference distilled water solution (0 ppm of Hg), it was possible to quantify the sensor's response to increasing concentrations of mercury chloride. This method provides a clearer view of the sensor's sensitivity to variations in concentration, highlighting the incremental changes in current as a function of the heavy metal concentration.

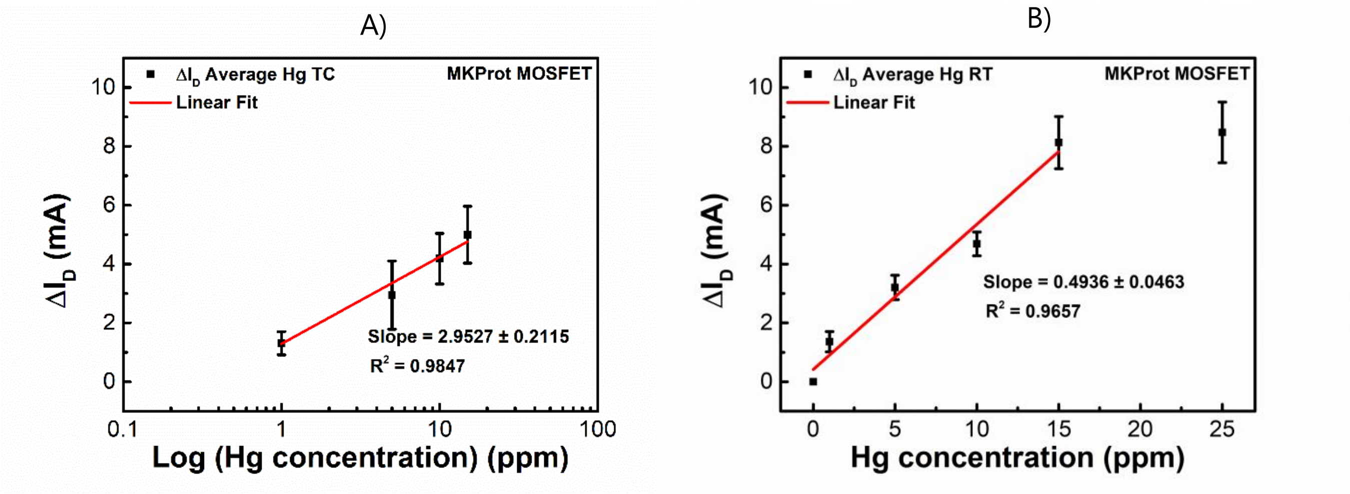

Figure 4.25: Sensitivity extracted for MKProt MOSFET from average ΔI_D for Hg solutions testing: A) from transfer curves; B) from real-time monitoring.

As observed in Figure 4.25, the increase in delta current with increasing Hg concentration is relatively consistent across both the transfer curve analysis and real-time monitoring. This consistency reinforces the sensor's sensitivity to lower concentrations of mercury chloride. In the real-time monitoring figure, the 15 ppm solution shows a more pronounced increase in ΔI_D compared to the transfer curves analysis. This difference can be attributed to the advantages of real-time analysis, as mentioned earlier. Real-time monitoring allows for immediate observation and manipulation of the sensor's behaviour, offering the ability to stabilize or adjust the testing conditions based on the sensor's live response.

As previously mentioned, for the real-time analyses, a 25 ppm solution was also tested, showing that the sensor does not exhibit any significant sensitivity beyond this concentration. This suggests a saturation point, where higher concentrations do not induce further measurable changes in the drain current.

Since the presented graphs show a non-linear relationship with the displayed values, especially for transfer curves analysis, the sensitivity was determined through a semi-log graph in the x-axis for the transfer curve analysis Figure 4.25.A), to obtain better fitting with a higher R^2, for this heavy metal. This way, a more accurate sensitivity measurement can be extracted. However, this way these extracted sensitivities can not be comparable to each other, registering for transfer curve analysis a sensitivity of 3.0 ± 0.2 mA/Log(ppm) and real-time monitoring, 0.49 ± 0.05 mA/ppm.

A similar plot was created by fixing the drain current values at approximately 70% of the maximum current observed in the transfer curve for each measurement, analogous to the pH measurement.

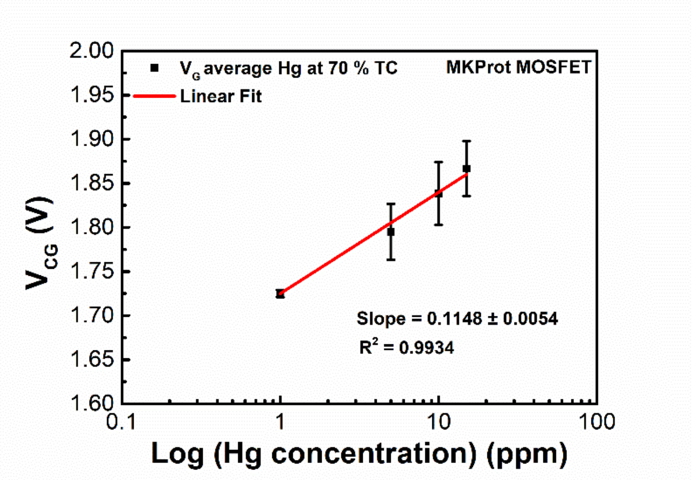

Figure 4.26: Sensitivity extracted for MKProt MOSFET at a fixed value of the transfer curve (70%) for Hg solutions testing.

From the linear fitting of the graph of Figure 4.26, it is possible to extract the sensitivity value in terms of voltage per concentration of heavy metal solution in ppm on a logarithmic scale. Thus, it is possible to record a value of 0.115 ± 0.005 mV/ppm when analyzing the established region between 1 ppm and 10 ppm.

4.2.3.2 Cadmium Chloride Solutions

For the measurements with cadmium solutions, it was determined that the sensor did not show significant sensitivity for concentrations below 1000 ppm. Therefore, the transfer curve and real-time analyses are presented in the following figures, using distilled water as a reference, along with the 1000 ppm and 3000 ppm solutions. These results highlight the sensor's response to higher concentrations of cadmium chloride, indicating its effectiveness within specific ranges, while lower concentrations were not sufficiently detected by the device.

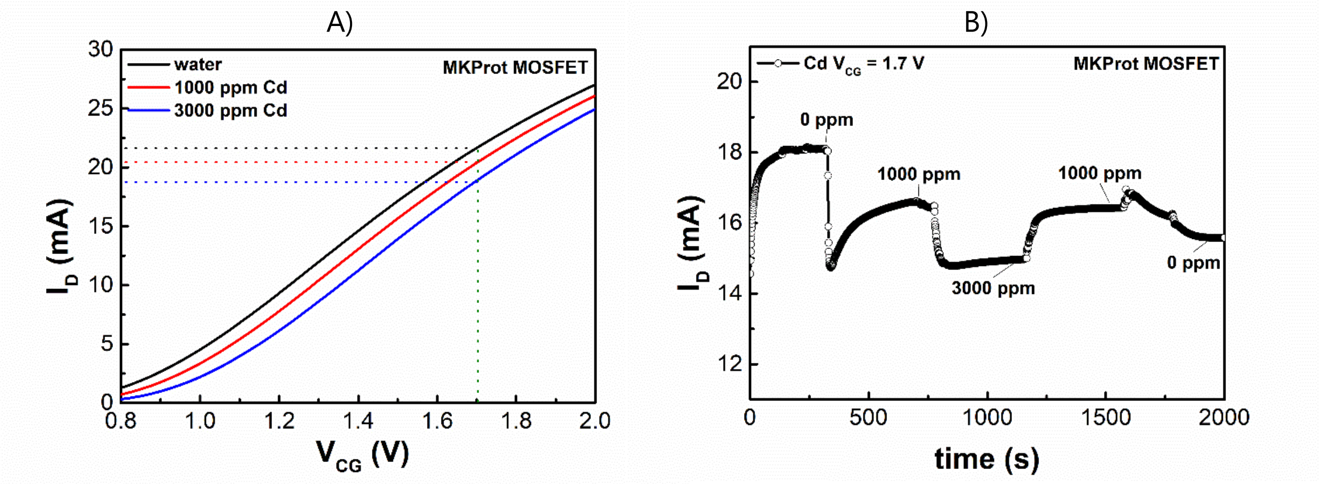

Figure 4.27: Cd solutions sensing performance of a tested sensor for MKProt MOSFET, evaluated through: A) transfer characteristics with V_D = 0.5 V; B) continuous real-time response of the drain current I_D at a fixed control gate voltage of V_{CG} = 1.7 V.

Through the graphs in Figure 4.27, a behaviour similar to what was previously recorded for mercury chloride can be observed. There is a decrease in the drain current as the concentration of cadmium solutions increases. This can be attributed to the accumulation of ions on the sensor's surface, which affects the charge modulation and results in the observed changes in current. This trend mirrors the sensor’s behaviour when exposed to heavy metals, highlighting its consistent response to positively charged ions.

As the real-time analysis in Figure 4.27.B) demonstrates, it is possible to observe a recovery of current when the concentration decreases. However, by the end of the measurements, significant wear of the sensor was consistently noted for all sensors, as it was not possible to recover the current value corresponding to the reference value of distilled water. This wear may be attributed to the accumulation of charges on the sensor's surface due to the high concentrations of solutions used in this analysis. The persistent exposure to elevated levels of cadmium ions likely led to saturation effects, hindering the sensor's ability to revert to its baseline state, thereby impacting its long-term performance and reliability. The following Figure 4.28 shows a sensor before and after heavy metal testing.

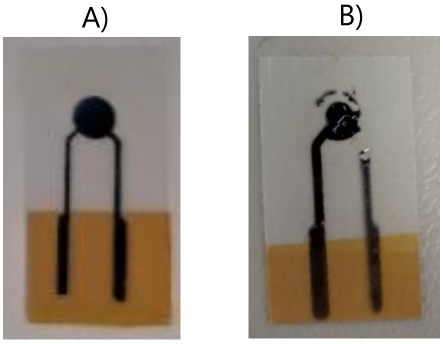

Figure 4.28: A) Sensor before testing; B) Sensor degradation after heavy metal (Cd) testing.

Similarly to the measurements conducted with mercury solutions, consecutive measurements on the same sensor were also not performed in this case due to the wear of the sensors, making it impossible to obtain a reliable response from the sensor. The degradation in sensor performance, attributed to the prolonged exposure to cadmium ions, resulted in a diminished ability to accurately measure subsequent concentrations. This limitation underscores the need for careful consideration of sensor longevity and recovery when developing detection methodologies for heavy metals in marine environments. Thus, the following analyses, conducted through transfer curve measurements and real-time monitoring, will demonstrate the average results for three different sensors.

The analysis of the sensor's behaviour in terms of current deltas for the different concentrations of Cd solutions is presented in the following images.

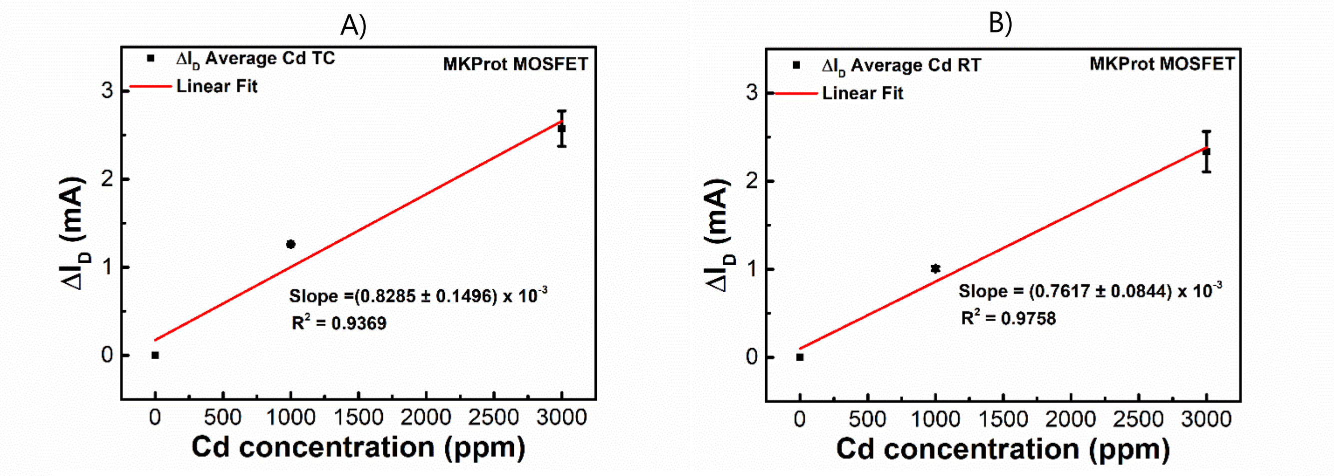

Figure 4.29: Sensitivity extracted for MKProt MOSFET from average ΔI_D for Cd solutions testing: A) from transfer curves; B) from real-time monitoring.

From the graphs in the previous Figure 4.29, it is extracted a sensitivity value of 0.8 ± 0.1 µA/ppm for transfer curve analysis, Figure 4.29.A), and 0.76 ± 0.08 µA/ppm for real-time monitoring, Figure 4.29.B). Contrary to expectations the sensitivity value for transfer curves analysis is higher than for real-time monitoring, however, it is noteworthy that these values are quite similar. Overall, the sensitivity of the sensor for cadmium solutions is relatively low, indicating a need for further optimization to enhance performance for this heavy metal.

Next, it is presented for this heavy metal the analysis of the extraction of the sensitivity in mV/ppm.

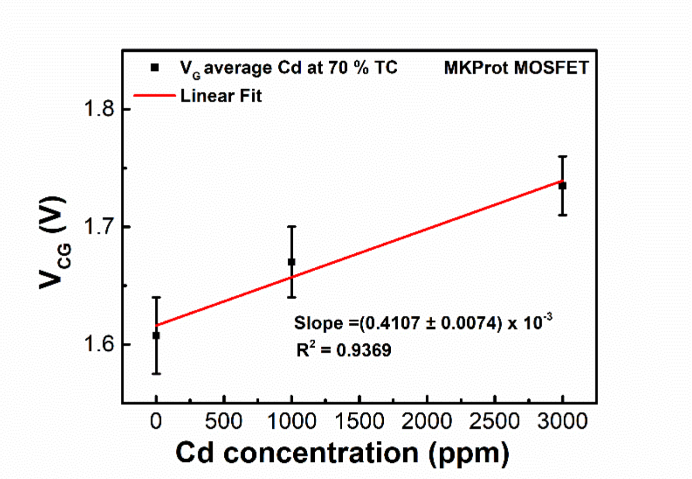

Figure 4.30: Sensitivity extracted for MKProt MOSFET at a fixed value of the transfer curve (70%) for Cd solutions testing.

From the linear fitting of the graph of Figure 4.30, it is possible to extract the sensitivity value in terms of voltage per concentration of heavy metal solution in ppm. Thus, it is possible to record a value of 0.411 ± 0.007 mV/ppm. This value is much lower than for the mercury solutions, as the sensor is capable of detecting mercury at concentrations as low as 1 ppm, potentially due to mercury's (Hg^{2+}) more favorable reduction potential (+0.851 V), which enables greater sensitivity in electrochemical detection. In contrast, cadmium (Cd^{2+}) requires much higher concentrations 1000-3000 ppm to produce a detectable response. This is likely due to cadmium's lower reduction potential (-0.4030V) [37] or potential interferences in the solution that hinder efficient detection at lower concentrations.

In Table 4.3 below, sensitivity values from all methodologies and the detection range determined are compiled to compare the two heavy metals tested.

Table 4.3: Summary of the sensitivities results obtained for both heavy metal testing (Hg and Cd solutions), detection range, LOD and WHO's permissive limit in drinking water

	Sensitivity TC ΔI_D	**Sensitivity RT ΔI_D**	**Sensitivity TC I_{REF} (mV/ppm)**	**Detection range (ppm)**	**Limit of Detection (LOD)**	**WHO's Permissive Limit**
Mercury Chloride (Hg)	3.0 ± 0.2 mA/Log(ppm)	0.49 ± 0.05 mA/pp,	0.115 ± 0.005 mV/Log(ppm)	1-15	1 ppm	0.001 ppm
Cadmium Chloride (Cd)	0.8 ± 0.2 µA/ppm	0.76 ± 0.08 µA/ppm	0.411 ± 0.007 mV/ppm	1000-3000	1000 ppm	0.003 ppm

As observed in Table 4.3, the only sensitivity value that can be directly compared for both heavy metals is the sensitivity extracted from the real-time analysis. This value was 3 orders higher for the detection of mercury than for cadmium solutions, indicating. The solubility of these compounds in water may explain the differentiated sensor behaviour for each heavy metal; cadmium chloride is much more soluble in water than mercury chloride, leading to easier precipitation of Hg^{2+} ions on the sensor's surface. Another reason could be that mercury, being a heavier and more reactive metal, may bind more effectively to the tantalum oxide surface compared to cadmium (Cd^{2+}). The sensor's behaviour may also be influenced by the point of zero charge (pHpzc) of tantalum oxide. If the pHpzc of Ta_2O_5 is closer to the conditions under which mercury is more reactive, it could promote a greater modification of the surface potential compared to cadmium.

The LOD for the sensor was lower for mercury solutions (1 ppm) compared to cadmium solutions (1000 ppm). However, when compared to the World Health Organization's (WHO) permissible limit in drinking water, the sensor's detection threshold for mercury is still three orders of magnitude higher, indicating that it is not yet suitable for detecting relevant concentrations of these metals, especially cadmium. Therefore, it is essential to optimize this process, particularly by improving the sensor's sensitive layer.

4.2.1 Analysis with Ag-NP Membranes

To determine the influence of modifying the sensor's sensitive layer, two preliminary analyses were conducted. The first focused on the sensor's behaviour when only Nafion was applied to the sensor surface, while the second analyzed the sensor's performance with membranes containing silver nanoparticles (Ag-NPs) deposited on the surface, using Nafion as the adhesion promoter (Figure 4.31). This approach aimed to leverage the unique properties of silver nanoparticles while using Nafion's conductive and selective characteristics to improve sensor performance. The incorporation of these materials allows for better interaction with target metal ions, leading to improved detection capabilities.

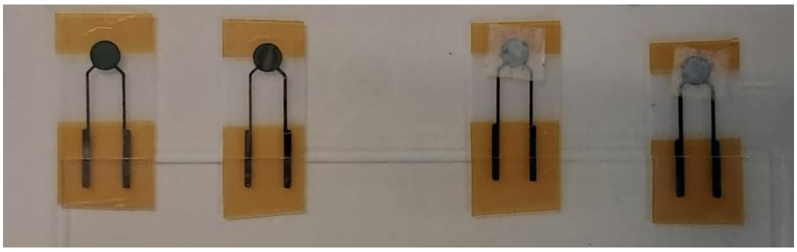

Figure 4.31: Sensors with Nafion deposited at the surface (right) and with Nafion and Ag-NPs membranes (left).

Firstly, the following Figure 4.32 presents the analysis conducted for two different sensors with varying quantities of Nafion deposited onto their surfaces - one with 10 µL and the other with 25 µL, tested with the same method as the previous analysis for pH solutions. This analysis aims to study the influence of Nafion quantity on the sensor's performance.

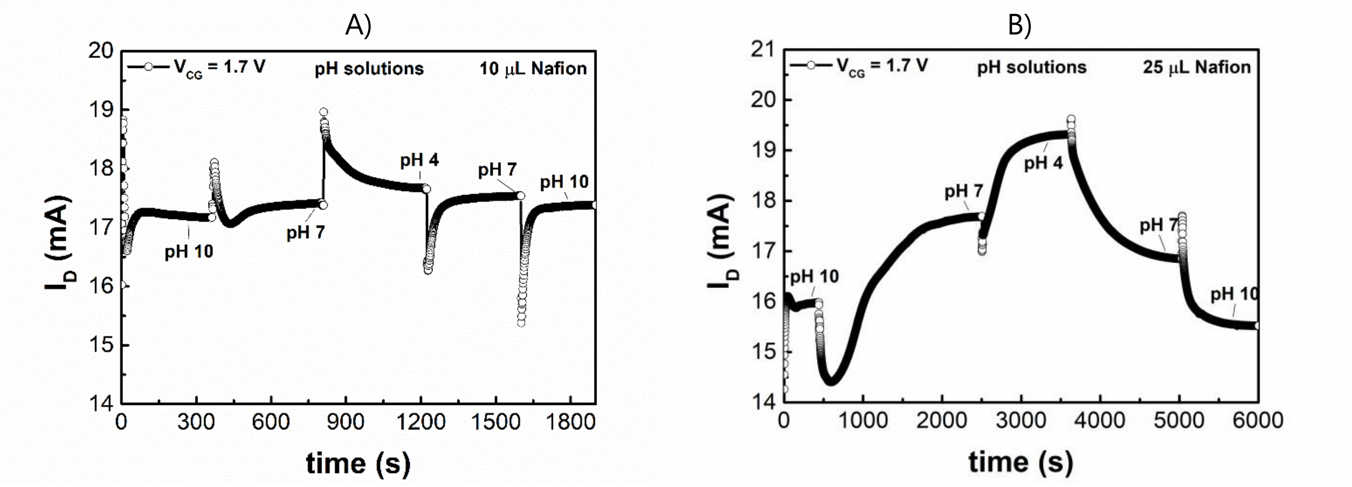

Figure 4.32: Real-time analysis for pH sensing in two different sensors whose surface was modified with; A) 10µL of Nafion deposited and B) 20µL of Nafion deposited.

As observed in the previous Figure 4.32, the sensors with Nafion on the surface remain responsive to pH differences, however, this response is inverted compared to what was expected from earlier analyses with pH solutions, even though the connections were maintained. This behaviour could be attributed to the electrical charge of Nafion. The sulfonate groups ($-SO_3^-$) impart a negative charge to Nafion when in contact with aqueous solutions. This occurs because the sulfonate groups dissociate into sulfonate ions (SO_3^-) and hydrogen ions (H^+) in solution, resulting in a net negative charge within the polymer matrix. [31]

For the sensor with less Nafion deposited, it is notable that there are no significant differences in current values between different pH buffers, in contrast to the sensor with a larger Nafion deposition. This difference can be linked to the electrical capacity of Nafion, however, the response time for the sensor with 25 µL of Nafion was approximately three times longer than that recorded for the sensor with 10 µL of Nafion deposited. This indicates that a greater quantity of Nafion on the surface may hinder charge transfer and reduce contact efficiency with the sensor, ultimately affecting its overall performance. The following Figure 4.33 shows the extracted sensitivities for these two measurements. The error bars are not displayed as repetitive measurements were not performed.

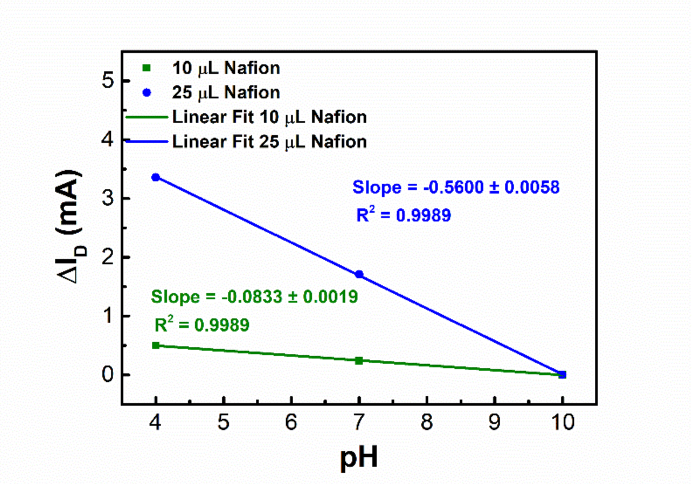

Figure 4.33: Sensitivity extracted for Nafion deposition from average ΔI_D for pH solutions testing: green) 10 µL of Nafion ; B) 25 µL of Nafion.

From this plot, in Figure 4.33, it's possible to confirm that the sensitivity for a larger deposition of Nafion is significantly higher (sensitivity= 0.560 ± 0.006 mA/pH) than the sensor with less Nafion deposited (sensitivity= 0.083 ± 0.002 mA/pH).

In the following, sensitivity values for pH testing in Agilent 4155C in real-time monitoring, with and without Nafion deposited onto the sensor's surface are registered to compare these results.

Table 4.4: Summary of sensitivity values extracted from real-time monitoring for pH testing in Agilent 4155C.

	Sensitivity RT ΔI_D (mA/pH
Without Nafion	1.14 ± 0.01 mA/pH
25 µL Nafion	0.560 ± 0.006 mA/pH
10 µL Nafion	0.083 ± 0.002 mA/pH

From Table 4.4, it is evident that the presence of Nafion, despite its conductive properties, significantly reduces the sensitivity of the sensor. The greater the amount of Nafion deposited, the lower the recorded sensitivity value. Although the sensitivity values for the sensors with Nafion may not be completely reliable due to the limited number of measurements performed, it provides a preliminary understanding of the behaviour of this compound on the sensor's surface. More extensive testing would be needed to confirm these observations.

The analysis of the sensor's performance with membranes containing silver nanoparticles (Ag-NPs) deposited on the surface, using Nafion as the adhesion promoter, was studied only with the solutions of mercury chloride. However, these did not show any sensitivity to the difference of concentration in these solutions, as it's possible to observe in the following Figure 4.34.

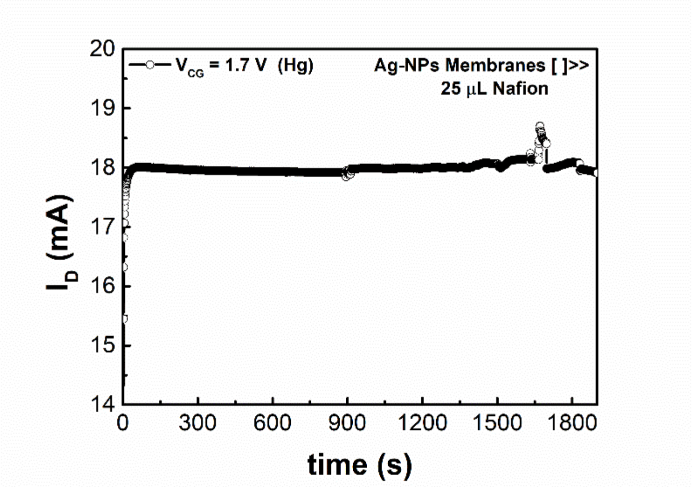

Figure 4.34: Real-time analysis for Hg testing in sensor with 25µL of Nafion and membranes with a higher concentration of Ag-NPs deposited.

As observed in Figure 4.34, there was no difference in the current recorded when varying the concentration of the mercury solution, and this finding was consistent across the other sensors characterized with membranes containing both concentrations of silver nanoparticles. This may be related to the membrane's inability to facilitate charge contact with the sensor's surface. This issue could also be linked to potential malfunctions in the tested sensors, as they originated from different batches. A failure in the manufacturing process might have occurred, contributing to variations in sensor performance and reliability. Such discrepancies could result in inconsistent outcomes for heavy metal detection. To address this, further investigation into the production process of these batches and the membrane composition is essential, ensuring consistent sensor quality and reliable performance. The transfer curves for this case were also conducted; however, they displayed an arbitrary order of appearance, with all curves overlapping each other.

To investigate the composition of the membranes and the distribution of nanoparticles to determine the cause, SEM and EDS analyses were performed.

4.3 Structural characterization of Ag-NPs membranes

To characterize the morphology and elemental composition of the membranes, two samples with different concentrations of Ag-NPs were analyzed using Scanning Electron Microscopy (SEM) and Energy Dispersive Spectroscopy (EDS). The analysis with mercury solutions (in Figure 4.34) was performed with the membrane with a higher concentration of Ag-NPs.

<The images obtained from the SEM analysis are presented in the next Figure 4.35 to examine the membrane's topography and composition, as SEM provides high-resolution surface imaging.

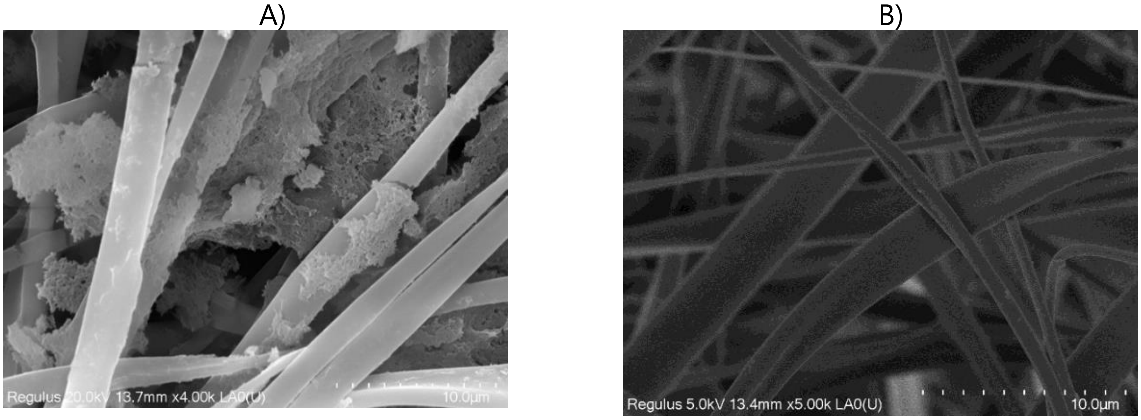

Figure 4.35: SEM images for membranes with; A) higher concentration of Ag-NPs; B) less concentration of Ag-NPs.

As observed in the images presented in Figure 4.35, particularly for the membrane with a higher concentration of nanoparticles, some elements, presumably from the Ag-NPs, can be seen adjacent to the fibers that make up the membrane. In contrast, the representative image of the membrane with a lower concentration of nanoparticles does not easily reveal these elements.

Despite the reliability and usefulness of SEM imaging, this technique does not provide information about the chemical elements present in the membranes beyond their topography. Therefore, EDS analysis was conducted to determine whether Ag-NPs were indeed present in the membrane composition, with the results presented in the following Figure 4.36.

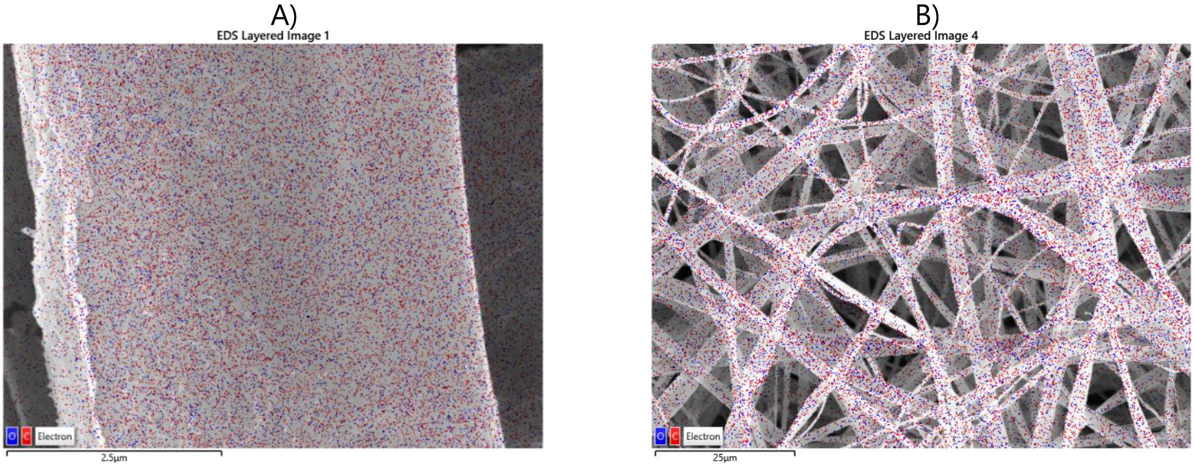

Figure 4.36: EDS images for membranes with; A) higher concentration of Ag-NPs; B) less concentration of Ag-NPs.

As observed in the images of Figure 4.36, the EDS analysis only detected carbon and oxygen in the membranes. However, for the membrane with the higher concentration, a close examination was performed on a specific fiber within the membrane. This may explain the inability to detect Ag-NPs, as they might not be uniformly distributed throughout the membranes. Consequently, the EDS analysis may not have provided a conclusive result regarding the presence of Ag-NPs. Therefore, further analyses of the membranes will be necessary to identify their constituents and uncover the reasons behind the unsuccessful detection of heavy metals. These additional investigations will provide valuable insights into the membrane composition and its interaction with the sensor, helping to clarify any underlying issues. Ultimately, this will enable the optimization of the detection process, ensuring that it becomes more reliable and effective for heavy metal detection.

5

CONCLUSIONS AND FUTURE PERSPECTIVES

This work focused on gathering data from sensors designed to detect pH levels and heavy metals, such as mercury and cadmium. Two different methodologies were employed to test pH solutions, to optimize a custom software system integrated with the developed PCB. The objective was to compare the data obtained from this custom system with the results from the laboratory's Agilent 4155C semiconductor parameter analyzer. This comparison was essential for evaluating whether the custom system could serve as a viable tool for detecting and quantifying heavy metals in aqueous solutions, aligning with the goals of the project.

The analyses using the Agilent 4155C system did not show a notable improvement in sensitivity in terms of voltage versus pH with the MKProt MOSFET compared to the commercial CD4007UB MOSFET. Sensitivity values of 40 ± 2 mV/pH and 39 ± 1 mV/pH were recorded for the MKProt and CD4007UB, respectively. However, when comparing the sensitivities extracted in terms of current per pH unit, there was an approximately 50-fold increase for the sensor with the MKProt MOSFET integrated and a much higher precision, registering a sensitivity of 23 ± 2 µA/pH for the commercial MOSFET and 1.14 ± 0.01 mA/pH for the developed MKProt. This enhancement is attributed to the signal amplification capability of the MKProt MOSFET, which exhibited a response in the milliampere range, significantly outperforming the CD4007UB's microampere range. Additionally, the use of an integrated microfluidic system connected to the sensor socket provided a substantial increase in sensitivity, with a registered value of 54 ± 1 mV/pH and 1.285 ± 0.003 mA/pH. compared to the manual solution deposition method. This sensitivity value in mV/pH is close to the theoretical limit. This improvement is largely due to the microfluidic system's advantages, including preventing direct contact with the sensor surface minimizing external interferences and ensuring a continuous, controlled flow of solution over the sensor, which enhances both accuracy and consistency in measurements.

The custom Controller board developed in the project was also tested against the Agilent 4155C SPA to confirm its viability for pH and future heavy metal measurements. The developed controller board demonstrated similar capabilities in differentiating between solutions when used with a resistance of 460Ω, registering a sensitivity value of 32.1 ± 0.8 mV/pH. This value is slightly lower than those determined by the method mentioned earlier, but still within the same order of magnitude, demonstrating its reliability. For future measurements, this resistance value could be adjusted as needed to suit specific measurement requirements. The custom software system presents several advantages over commercially available options, as it is precisely tailored to meet the unique needs of in-situ detection for this project. This customization ensures that the software integrates seamlessly with the sensor system, offering flexibility and optimization for ongoing and future heavy metal detection tasks.

In the laboratory analyses conducted for heavy metal detection, the sensor demonstrated better sensitivity towards mercury ions than cadmium ions. Specifically, for mercury chloride ($HgCl_2$) solutions, the sensor was able to detect concentrations within the range of 1-15 ppm, which aligns with realistic environmental contamination levels, making the sensor potentially useful for detecting mercury in practical applications, such as in water quality monitoring.

However, when it came to cadmium chloride ($CdCl_2$) solutions, the detection range was considerably less favourable, with the sensor only responding to concentrations between 1000-3000 ppm. This range is much higher than the typical cadmium ion concentrations found in natural water bodies, where cadmium levels are usually in the ppb (parts per billion) range or lower. Such elevated detection thresholds make the sensor unsuitable for cadmium detection in environmental monitoring. This could be due to several factors, including the sensor's material properties, the interaction of cadmium ions with the sensitive layer, or the electrochemical characteristics of the metal ions. Therefore, additional optimizations, such as modifying the sensitive layer or incorporating selective membranes, would be necessary to improve the sensor's performance for cadmium detection.

For this reason, two types of preliminary analyses were conducted to try to optimize the detection and sensitivity of the sensors for these heavy metals. The first analysis involved applying Nafion to the surface of two sensors, which were then tested with pH solutions to understand the influence of this conductive polymer on sensor performance. It was observed that the sensor with a higher amount of Nafion deposited exhibited greater sensitivity, but also showed a longer response time. This suggests that while Nafion can improve sensitivity, the increased thickness may hinder charge transfer, leading to delayed response times. The second analysis focused on sensors with membranes containing silver nanoparticles (Ag-NPs), which were tested with heavy metal solutions. However, the sensors displayed no detectable sensitivity to changes in the heavy metal solutions, which was unexpected. The lack of sensitivity could be due to several factors, including the distribution of Ag-NPs within the membrane or potential issues with the interaction between the membrane and the sensor surface.

These preliminary tests were not entirely conclusive regarding the behaviour of the Nafion and Ag-NP membranes. One key limitation was that repeated tests were not conducted on each sensor, leaving open the possibility that the results were influenced by sensor inconsistencies. This is particularly relevant as the sensors used in these tests came from an untested batch, meaning that a manufacturing defect could have affected their performance. Further testing and validation are necessary to confirm these findings and to better understand the role of these materials in enhancing sensor sensitivity for heavy metal detection.

From all the tests conducted, it is evident that real-time analyses offer significant advantages over transfer curves or voltage sweeps (as performed with the developed controller board). Real-time analysis proves to be more accurate and reliable for data acquisition, demonstrating higher sensitivity values and smaller associated errors. In most cases, real-time measurements provided improved signal-to-noise ratios, making real-time monitoring particularly beneficial for applications requiring precise and continuous detection of heavy metals in flowing water systems, including rivers and seas, where small variations in concentration need to be captured efficiently.

In future perspectives, it is crucial to extend these analyses to a broader range of heavy metals and determining the influence of salinity in water, testing the sensors using the custom software system and PCB designed for this project to confirm their reliability in such measurements. One measurement that was not possible to perform involved using the microfluidic system in conjunction with the custom software and PCB, as this apparatus induced significant interference in the measured signal. The interference was likely due to the mechanical vibrations of the microfluidic device, which created noise that the software system, being highly sensitive to both external and internal disturbances, could not filter out effectively.

To prevent the physical wear of the sensors, which was a recurring issue during heavy metal testing, certain measures could be incorporated into the fabrication process. For instance, adding a protective parylene coating could help shield the sensor's contacts, ensuring durability and more reliable long-term use. This protective layer would not only help safeguard the sensor during measurements but also enhance its overall robustness when exposed to corrosive or high-concentration heavy metal solutions.

In an eco-friendlier approach, it would also be beneficial to test and optimize sensors made from different types of substrates, such as paper. Paper-based sensors offer several advantages, including low-cost production, biodegradability, and the potential for disposable applications, which can significantly reduce environmental impact. Research into paper-based sensors could focus on their sensitivity and selectivity for heavy metals, exploring various coating materials and modification techniques to enhance their performance.

BIBLIOGRAPHY

[1] "Goal 14 | Department of Economic and Social Affairs." [Online]. Available: https://sdgs.un.org/goals/goal14.

[2] "Almost 1 million people die every year due to lead poisoning, with more children suffering long-term health effects." . Available: https://www.who.int/news/item/23-10-2022-almost-1-million-people-die-every-year-due-to-lead-poisoning--with-more-children-suffering-long-term-health-effects.

[3] M. Balali-Mood, K. Naseri, Z. Tahergorabi, M. R. Khazdair, and M. Sadeghi, "Toxic Mechanisms of Five Heavy Metals: Mercury, Lead, Chromium, Cadmium, and Arsenic," *Front. Pharmacol.*, vol. 12, Apr. 2021, doi: 10.3389/FPHAR.2021.643972.

[4] N. Narwal *et al.*, "Emerging micropollutants in aquatic ecosystems and nanotechnology-based removal alternatives: A review," *Chemosphere*, vol. 341, Nov. 2023, doi: 10.1016/J.CHEMOSPHERE.2023.139945.

[5] S. Mitra *et al.*, "Impact of heavy metals on the environment and human health: Novel therapeutic insights to counter the toxicity," *J. King Saud Univ. - Sci.*, vol. 34, no. 3, p. 101865, Apr. 2022, doi: 10.1016/J.JKSUS.2022.101865.

[6] W.-K. Lee, F. Thévenod, · Elmar, and J. Prenner, "Global threat posed by metals and metalloids in the changing environment: a One Health approach to mechanisms of toxicity," *Biometals*, vol. 1, pp. 539–544, 123AD, doi: 10.1007/s10534-024-00606-0.

[7] "Guidelines for Drinking-water Quality FOURTH EDITION WHO Library Cataloguing-in-Publication Data Guidelines for drinking-water quality-4 th ed," 2011.

[8] W. Tawfik, M. El-Saeed, A. Khalil, and M. Fikry, "Detection of heavy metal elements by using advanced optical techniques," *J. Egypt. Soc. Basic Sci.*, vol. 0, no. 0, pp. 99–127, Mar. 2024, doi: 10.21608/JESBSP.2024.255191.1002.

[9] C. Liu, Z. Ye, X. Wei, and S. Mao, "Recent advances in field-effect transistor sensing strategies for fast and highly efficient analysis of heavy metal ions," *Electrochem. Sci. Adv.*, vol. 2, no. 5, pp. 1–16, 2022, doi: 10.1002/elsa.202100137.

[10] M. D. Shirsat and T. Hianik, "Electrochemical Detection of Heavy Metal Ions Based on Nanocomposite Materials," *J. Compos. Sci.*, vol. 7, no. 11, 2023, doi: 10.3390/jcs7110473.

[11] T. Manimekala, · R Sivasubramanian, and · Gnanaprakash Dharmalingam, "Nanomaterial-Based Biosensors using Field-Effect Transistors: A Review," *J. Electron. Mater.*, vol. 51, pp. 1950–1973, 1234, doi: 10.1007/s11664-022-09492-z.

[12] X. Ma, R. Peng, W. Mao, Y. Lin, and H. Yu, "Recent advances in ion-sensitive field-effect transistors for biosensing applications," *Electrochem. Sci. Adv.*, vol. 3, no. 3, p. e2100163, Jun. 2023, doi: 10.1002/ELSA.202100163.

[13] D. Mudusu *et al.*, "Metal–insulator–semiconductor field-effect transistors (MISFETs) using p-type SnS and nanometer-thick Al2S3 layers," *RSC Adv.*, vol. 7, no. 18, pp. 11111–11117, Feb. 2017, doi: 10.1039/C7RA00041C.

[14] R. Branquinho "Label-free detection of biomolecules with Ta 2 O 5 -based field effect devices." 2012, PhD thesis, NOVA University FCT-UNL, Lisbon.

[15] J. Zou *et al.*, "Ion-sensitive field effect transistor biosensors for biomarker detection: current progress and challenges," *J. Mater. Chem. B*, vol. 12, no. 35, pp. 8523–8542, Sep. 2024, doi: 10.1039/D4TB00719K.

[16] S. Casans, D. R. Muñoz, A. E. Navarro, and A. Salazar, "ISFET drawbacks minimization using a novel electronic compensation," *Sensors Actuators, B Chem.*, vol. 99, no. 1, pp. 42–49, 2004, doi: 10.1016/j.snb.2003.09.015.

[17] S. Jamasb, S. Collins, and R. L. Smith, "A physical model for drift in pH ISFETs," *Sensors Actuators, B Chem.*, vol. 49, no. 1–2, pp. 146–155, 1998, doi: 10.1016/S0925-4005(98)00040-9.

[18] M. Bartošík *et al.*, "Mechanism and Suppression of Physisorbed-Water-Caused Hysteresis in Graphene FET Sensors," *ACS Sensors*, vol. 5, no. 9, pp. 2940–2949, Sep. 2020, doi: 10.1021/acssensors.0c01441.

[19] B. Veigas *et al.*, "Ion sensing (EIS) real-time quantitative monitorization of isothermal DNA amplification," *Biosens. Bioelectron.*, vol. 52, pp. 50–55, Feb. 2014, doi: 10.1016/J.BIOS.2013.08.029.

[20] M. Barbaro, A. Bonfiglio, and L. Raffo, "A charge-modulated FET for detection of biomolecular processes: Conception, modeling, and simulation," *IEEE Trans. Electron Devices*, vol. 53, no. 1, pp.

158–166, 2006, doi: 10.1109/TED.2005.860659.

[21] B. Veigas *et al.*, “Quantitative real-time monitoring of RCA amplification of cancer biomarkers mediated by a flexible ion sensitive platform,” *Biosens. Bioelectron.*, vol. 91, pp. 788–795, 2017, doi: 10.1016/j.bios.2017.01.052.

[22] G. Felix ”Production and electrical characterization of microsensors for marine mutagens and carcinogens monitoring", 2022, Msc thesis, NOVA University FCT-UNL, Lisbon.

[23] X. Y. Lin, Y. X. Liu, Y. J. Zhang, H. M. Shen, and Y. Guo, “Polycyclic aromatic hydrocarbon exposure and DNA oxidative damage of workers in workshops of a petrochemical group,” *Chemosphere*, vol. 303, p. 135076, Sep. 2022, doi: 10.1016/J.CHEMOSPHERE.2022.135076.

[24] S. Falina *et al.*, “Ten Years Progress of Electrical Detection of Heavy Metal Ions (HMIs) Using Various Field-Effect Transistor (FET) Nanosensors: A Review,” *Biosens. 2021, Vol. 11, Page 478*, vol. 11, no. 12, p. 478, Nov. 2021, doi: 10.3390/BIOS11120478.

[25] S. Sinha and T. Pal, “A comprehensive review of FET-based pH sensors: materials, fabrication technologies, and modeling,” *Electrochem. Sci. Adv.*, vol. 2, no. 5, p. e2100147, Oct. 2022, doi: 10.1002/ELSA.202100147.

[26] X. Liu, L. Huang, and K. Qian, “Nanomaterial-Based Electrochemical Sensors: Mechanism, Preparation, and Application in Biomedicine,” *Adv. NanoBiomed Res.*, vol. 1, no. 6, p. 2000104, Jun. 2021, doi: 10.1002/ANBR.202000104.

[27] F. Sudarman, · M Shiddiq, · B Armynah, and · D Tahir, “Silver nanoparticles (AgNPs) synthesis methods as heavy-metal sensors: a review,” *Int. J. Environ. Sci. Technol.*, vol. 20, no. 3, pp. 9351–9368, 2023, doi: 10.1007/s13762-022-04745-0.

[28] A. Waheed, M. Mansha, and N. Ullah, “Nanomaterials-based electrochemical detection of heavy metals in water: Current status, challenges and future direction,” *TrAC Trends Anal. Chem.*, vol. 105, pp. 37–51, Aug. 2018, doi: 10.1016/J.TRAC.2018.04.012.

[29] S. Gupta, N. George, M. Yadav, and V. Dwibedi, “Optical detection of heavy metal contaminants: advancements with bio-functionalized gold nanoparticles in environmental monitoring,” *Chem. Pap. 2023 782*, vol. 78, no. 2, pp. 699–714, Oct. 2023, doi: 10.1007/S11696-023-03145-Z.

[30] S. A. F. Kusuma, J. A. Harmonis, R. Pratiwi, and A. N. Hasanah, “Gold Nanoparticle-Based Colorimetric Sensors: Properties and Application in Detection of Heavy Metals and Biological Molecules,” *Sensors 2023, Vol. 23, Page 8172*, vol. 23, no. 19, p. 8172, Sep. 2023, doi: 10.3390/S23198172.

[31] F. A. Zakil, S. K. Kamarudin, and S. Basri, “Modified Nafion membranes for direct alcohol fuel cells: An overview,” *Renew. Sustain. Energy Rev.*, vol. 65, pp. 841–852, Nov. 2016, doi: 10.1016/j.rser.2016.07.040.

[32] M. Kim, J. Park, H. Park, W. Jo, W. Lee, and J. Park, “Detection of Heavy Metals in Water Environment Using Nafion-Blanketed Bismuth Nanoplates,” *ACS Sustain. Chem. Eng.*, vol. 11, no. 18, pp. 6844–6855, May 2023, doi: 10.1021/ACSSUSCHEMENG.2C05263/SUPPL_FILE/SC2C05263_SI_001.PDF.

[33] M. Alvarez,” Optimization of a controller for marine pollutant monitoring using field effect devices", 2023, Msc thesis, NOVA University FCT-UNL, Lisbon

[34] G. Mills and G. Fones, “A review of in situ/IT methods and sensors for monitoring the marine environment,” *Sens. Rev.*, vol. 32, no. 1, pp. 17–28, 2012, doi: 10.1108/02602281211197116.

[35] N. Sharma, M. Kumar, N. Kumari, A. Deep, J. K. Goswamy, and A. L. Sharma, “Tantalum oxide thin films for electrochemical pH sensor,” *Mater. Res. Express*, vol. 7, no. 3, p. 036405, Mar. 2020, doi: 10.1088/2053-1591/AB7CED.

[36] D. Chen, C. Dong, J. Pan, G. R. Engelhardt, and D. D. Macdonald, “Development of the General Methodology for Determining the Point of Zero Charge of Oxide Films by Contact Angle Titration,” *J. Electrochem. Soc.*, vol. 170, no. 8, p. 081504, Aug. 2023, doi: 10.1149/1945-7111/ACEDD2.

[37] D. B. Short *et al.*, “Fast food premium toys as a significant source of lead and chromium to the environment,” *J. Toxicol. Environ. Heal. Sci.*, vol. 8, no. 7, pp. 68–75, Dec. 2016, doi: 10.5897/JTEHS2016.0373.

A

APPENDIX

A.1 Sensor Fabrication

The CMISFET sensor proposed consists basically of 4 different layers deposited sequentially in a PEN substrate. For the substrates, an overnight thermal treatment was performed, placed in an oven at 150°C, and after this step was submitted to a cleansing process involving 10 minutes in ultrasonic bath of acetone, followed by 10 minutes of ultrasonic bath in isopropyl alcohol and rinsed with ultra-pure water. Most of the ultra-pure water was carefully removed with a nitrogen gun, and in the final step, the substrates were placed in a hotplate for 20 minutes at a temperature of 120°C to make sure any left cleansing products were evaporated.

These layers of the sensor consist of bottom and top contacts, dielectric and sensitive layer, that have different deposition methods. Before to each thin film deposition, each layer can be patterned by aligning a physical mask. The back and front contacts are both made of 60 nm thick molybdenum thin films that were sputtered in an AJA-ATC-1800 F system using a 3" target (3 mm thick, 99.95% purity; Alineason Materials Technology, Germany) with a deposition pressure of 0.23 Pa (1.7 mTorr), in an argon atmosphere (Ar = 50 sccm), and rf power of 175 W to achieve a uniform layer deposition in substrates.

The dielectric layer can be obtained by chemical vapour deposition (CVD) of Parylene-C (deposited in two sequential steps of 0.3g) using a Speciality Coating PDS-2010 Parylene coater using silane as an adhesion promoter, to obtain a ~400 nm dielectric layer. Stand-ard deposition parameters were used: furnace temperature of 690 °C; pressure gauge temperature of 135 °C; vaporizer temperature of 175 °C at a pressure of 1.87 Pa (14 mTorr)

The sensitive layer made with tantalum oxide (Ta_2O_5) thin films can be deposited using sputtering, similar to the molybdenum layer with a 3" (7.62 cm) Ta_2O_5 ceramic target (99.99% purity; Alineason Materials Technology, Germany) and deposited with a thickness of ~100 nm. Before deposition, pre-sputtering (sputtering with the shutter closed to prevent deposition) was performed for 10 min to ensure thin film reproducibility. For this step, deposition pressure of 0.3 Pa (2.3 mTorr), deposition gases ratio (Ar: O_2) of 14:0.5 sccm, and rf power of 150 W were used.

Regarding the sensor's fabrication, the layer's deposition sequence can be observed in a stacked configuration in Figure 5.1.

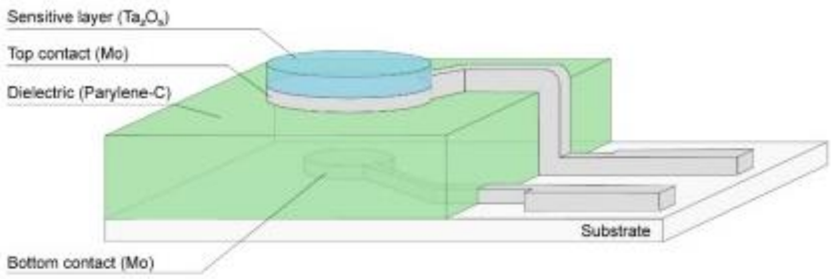

Figure 5.1: CMISFET sensor fabrication in a stacked configuration with all layers

A.2 Physical masks used for thin film deposition

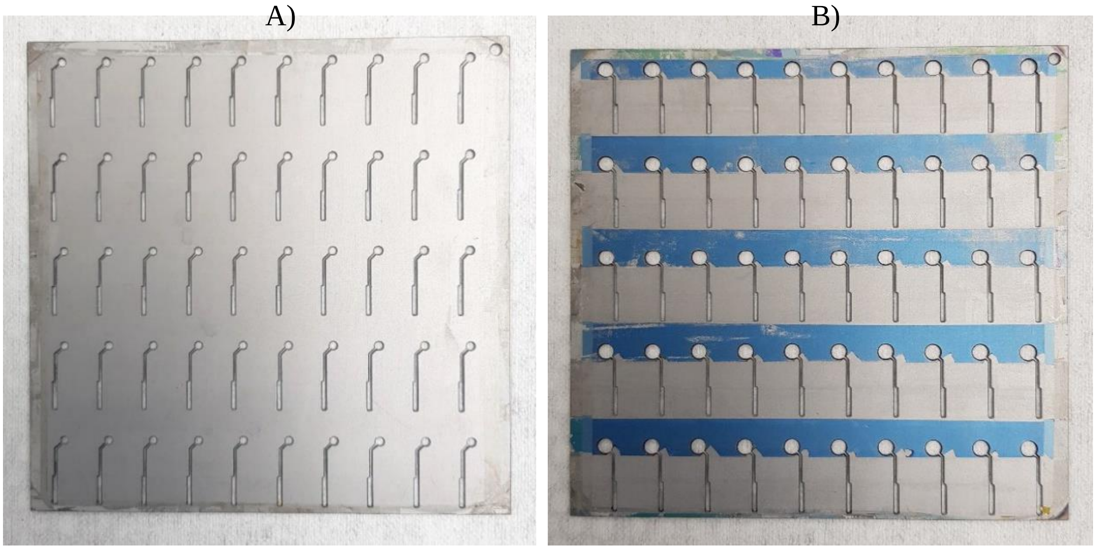
A)

B)

Figure 5.2: Physical masks used for sensor fabrication. (A) mask for bottom Mo contact layer deposition. (B) mask for bottom Mo contact and sensitive Ta_2O_5 layer depositions.

A.3 Sensor Batches

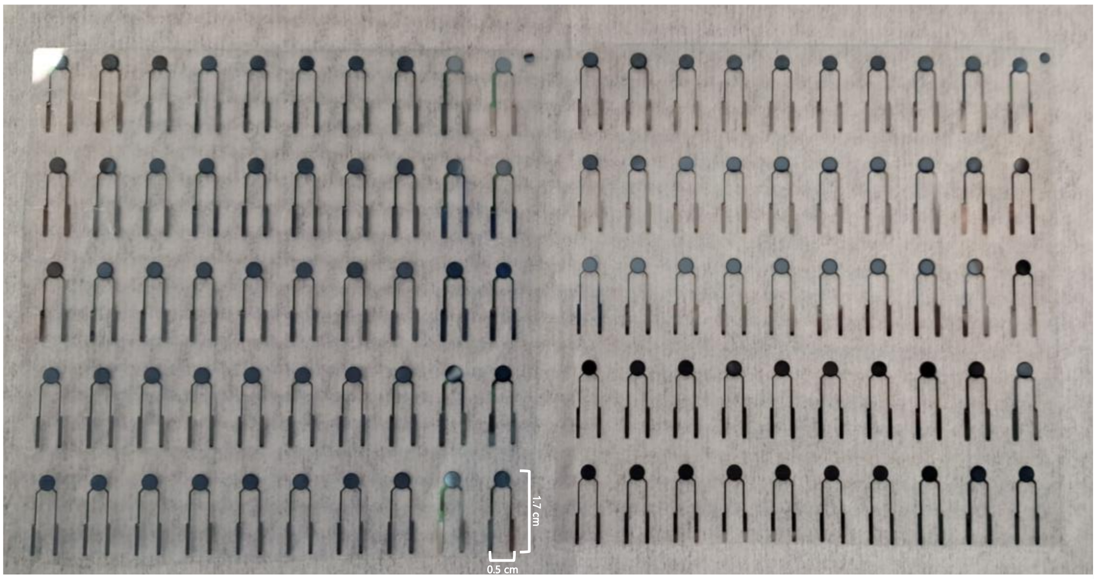

Figure 5.3: Batches of sensors produced on PEN substrate

A.4 Schematic diagram of Custom-PCB

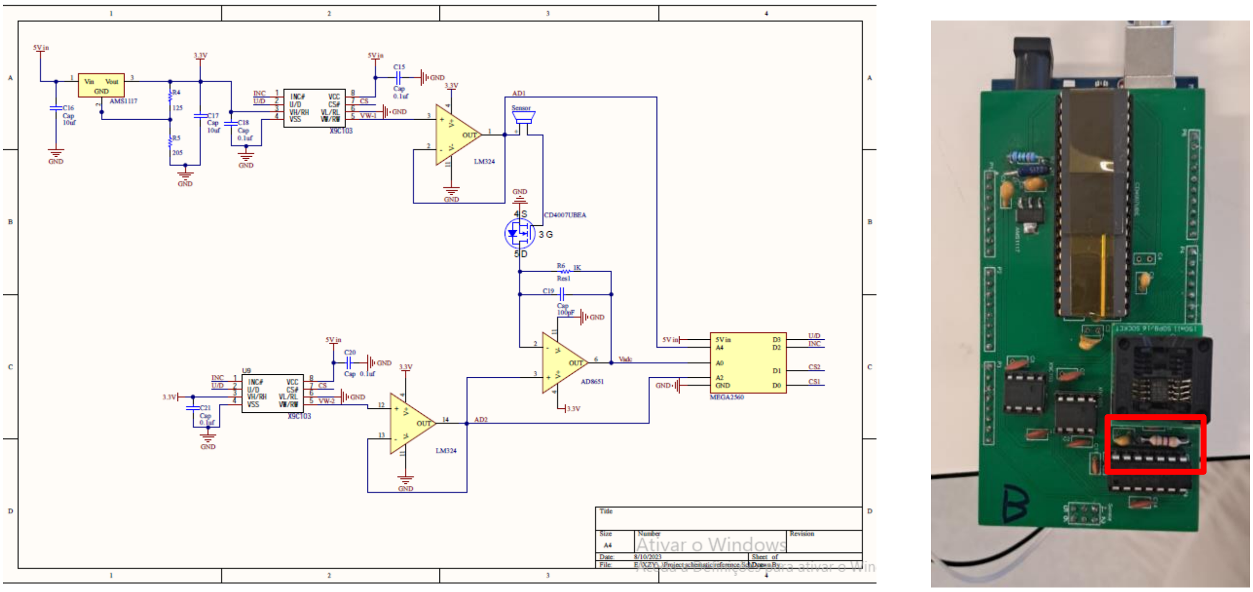

Figure 5.4: Custom-PCB; A) Schematic diagram; B) PCB with changeable resistor marked in red rectangle.

A.5 Sensor batches capacitance dry tests

Table 5.1: Sensor batch 1 in PEN substrates, with capacitance values (C) in nF and Dissipation Factor (D)

C (nF) D factor	1	2	3	4	5	6	7	8	9	10
A	154 0.051	151 0.051	151 0.050	>	150 0.049	149 0.109	150 0.049	172 0.051	250 0.058	189 0.051
B	139 0.059	150 0.051	144 0.050	148 0.058	168 0.056	165 0.053	152 0.052	170 0.054	216 0.058	213 0.061
C	>	165 0.065	154 0.052	156 0.058	165 0.065	>	157 0.052	205 0.058	250 0.050	>
D	147 0.050	>	>	159 0.053	159 0.053	203 0.057	172 0.054	210 0.058	281 0.060	263 0.061
E	165 0.053	216 0.050	210 0.057	173 0.054	>	189 0.058	185 0.055	217 0.057	>	>

Working sensors: 80%

Average Capacitance: 180 ± 35 nF

Average Dissipation Factor: 0.055 ± 0.004

Table 5.2: Sensor batch 2 in PEN substrates, with capacitance values (C) in nF and Dissipation Factor (D)

C (nF) D factor	1	2	3	4	5	6	7	8	9	10
A	154 0.050	154 0.049	156 0.051	149 0.051	149 0.051	148 0.050	154 0.050	174 0.050	258 0.058	>
B	136 0.050	149 0.051	159 0.053	172 0.056	197 0.057	180 0.057	152 0.049	173 0.053	>	?
C	?	168 0.056	179 0.057	191 0.058	203 0.059	212 0.058	172 0.052	215 0.059	>	253 0.060
D	173 0.054	201 0.057	187 0.057	173 0.059	170 0.054	218 0.060	178 0.056	236 0.051	317 0.063	>
E	177 0.054	222 0.058	201 0.058	174 0.053	>	>	187 0.056	>	>	202 0.059

Working sensors: 80%

Average Capacitance: 186 ± 35 nF

Average Dissipation Factor: 0.055 ± 0.004

Table 5.3: Sensor batch 2 in PEN substrates, with capacitance values (C) in nF and Dissipation Factor (D)

C (nF) D factor	1	2	3	4	5	6	7	8	9	10
A	143 0.046	>	>	126 0.045	?	126 0.049	127 0.042	161 0.054	262 0.053	190 0.049
B	>	152 0.046	138 0.051	139 0.046	148 0.046	137 0.045	133 0.043	160 0.047	219 0.052	>
C	>	161 0.059	146 0.048	140 0.047	143 0.046	>	134 0.043	184 0.050	?	221 0.053
D	126 0.044	157 0.050	139 0.201	129 0.045	132 0.044	>	>	>	238 0.053	225 0.053
E	134 0.043	157 0.045	147 0.045	133 0.042	132 0.044	151 0.046	157 0.046	175 0.047	256 0.052	>

Working sensors: 74%

Average Capacitance: 161 ± 37 nF

Average Dissipation Factor: 0.048 ± 0.004

Table 5.4: Sensor batch 4 in PEN substrates, with capacitance values (C) in nF and Dissipation Factor (D)

C (nF) D factor	**1**	**2**	**3**	**4**	**5**	**6**	**7**	**8**	**9**	**10**
A	128 0.046	138 0.048	168 0.050	199 0.050	218 0.048	201 0.050	141 0.048	156 0.046	225 0.057	>
B	132 0.051	147 0.048	163 0.053	169 0.053	169 0.051	175 0.056	155 0.049	160 0.047	189 0.051	186 0.052
C	146 0.049	160 0.050	150 0.050	124 0.042	142 0.049	149 0.050	135 0.046	>	>	>
D	?	158 0.144	139 0.049	124 0.045	131 0.046	176 0.052	164 0.051	218 0.057	300 0.063	>
E	141 0.047	170 0.051	153 0.050	128 0.048	133 0.048	179 0.059	202 0.057	240 0.058	324 0.069	256 0.159

Working sensors: 84%

Average Capacitance: 170 ± 43 nF

Average Dissipation Factor: 0.051 ± 0.005

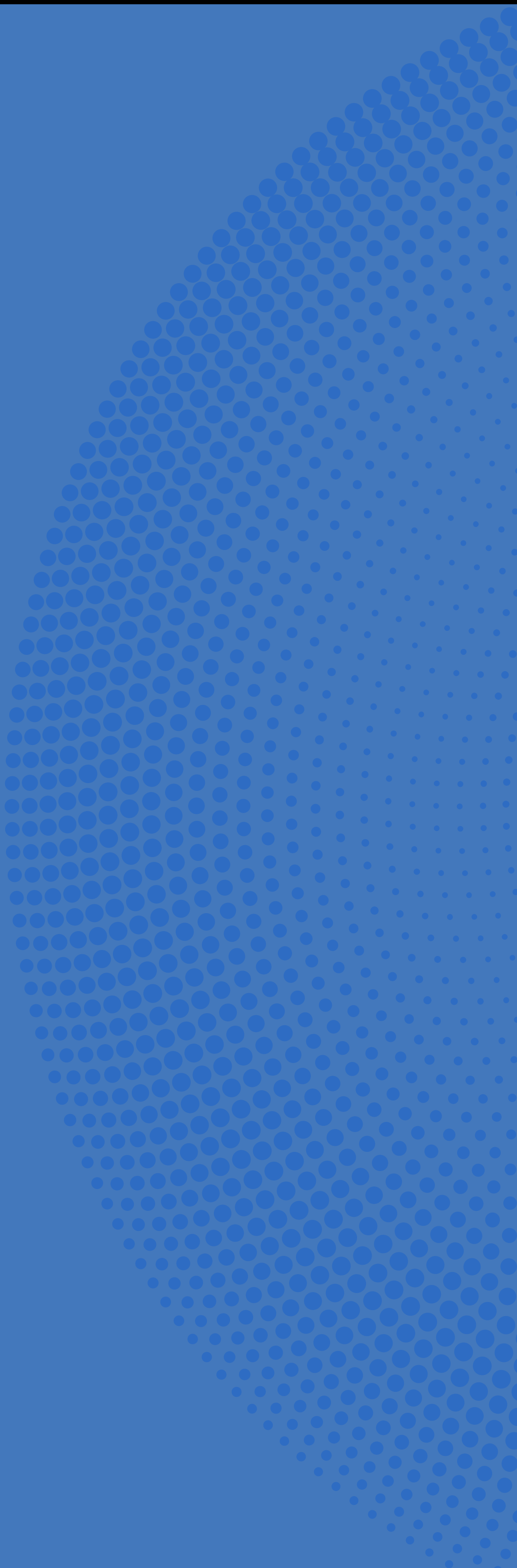

2024

Carolina Parreira

Integration of a new sensing controller for marine pollutant monitoring using field effect devices

NOVA SCHOOL OF
SCIENCE & TECHNOLOGY